

Mobile Government Next Generation as Development Gateway to M-services

Raheem Abudl Sahib Oglia Hussein Bader
Ministry of Science and Technology / Directorate of Information Technology
Baghdad_Iraq
Email: rrzmtl@yahoo.com

Abstract

This research aims to use the mobile device to access the applications and web services which are available on E-government portal by using private local network (intranet). Mobile network, mobile devices and mobile services are developed which construct the M-government in order to extend the horizon of online government services and maximize benefits from e-services. The suggested m-government used Wimax Technology as media based the framework of open source operating system. The main targets of our work are to provide more power security for the information that exchange through intranet, the cost of infrastructure will reduced against that is in ordinary E-government and the added value of our work to support peoples those are live courtyard to uses e-services. In the practical side we design a prototype of m-PORTAL and MSC (mobile switching center) to prove our concept.

Keywords: M-government, e-government, Mportal, M-Services and Mobile Switching Center

الحكومة الجواله الجيل القادم لتطوير بوابة خدمات الهاتف النقال

رحيم عبد الصاحب عكله حسين بدر حمدالله
وزارة العلوم والتكنولوجيا / دائرة تكنولوجيا المعلومات
بغداد - العراق

الخلاصة

يهدف البحث إلى استخدام جهاز الموبايل للوصول إلى تطبيقات وخدمات الويب المتوفرة على بوابة الحكومة الالكترونية باستخدام الشبكة المحلية الخاصة (الانترانيت) والتي تعتمد على تقنية Wimax وتعتمد تلك الخدمات والتطبيقات على بنية المصدر المفتوح وعدم استخدام شبكات الهاتف النقال العاملة. وقد استهدف البحث توفير أمنية عالية للمعلومات المتناقلة عبر شبكة اللاسلكية وتقليل الكلف فيما يخص البني التحتية للحكومة الالكترونية والاستفادة الأكثر أهمية من نتائج البحث من خلال استخدام الهاتف النقال في المناطق النائية مثل القرى والأرياف. في الجانب العملي تم تصميم نموذج بوابة الكترونية لغرض إثبات فكرة البحث.
الكلمات المفتاحية: الحكومة الجواله، الحكومة الالكترونية، بوابة الهاتف النقال، الخدمات الالكترونية.

Introduction

E-government efforts aim to benefit from the use of most innovative forms of information technologies, particularly web-based Internet applications, in improving governments' fundamental functions. These functions are now spreading the use of mobile and wireless technologies and creating a new direction of mobile government (m-government). M-government is defined as the strategy and its implementation involving the utilization of all kinds of wireless and mobile technology, services, applications and devices for improving benefits to the parties involved in e-government including citizens, businesses and all government units (Al Thunibat, 2010) Mobile e-government is a new e-government application model that develops on the basis of traditional e-government. It mainly utilizes mobile termination (MT) to have real-time access to e-government platform through mobile communication wireless network, in order to realize real time information interaction between civil servants in governments and the general public. This kind of model can adequately break the double limits of time and region, and provide convenient mobile e-government information services for all levels of governments, enterprises and public institutions, social

groups and the general public (Mukherjee,2005)(Shahkooh ,2007).

Today, the use and the development of wireless web technology (e.g. portal technology running on wireless handheld devices)

(Zarei,2008) (Garcia,2005) (Andersen ,2006) are reaching to critical mass, and we are witnessing an explosion in the use of wireless Internet appliances, including Internet-ready mobile phones and Personal Digital Assistants (PDAs). While citizens' access to government information and services are driving force for developing new applications and enhancing existing applications; handheld devices and wireless access can enhance the work performance of government workers to give better services to citizens/clients (Nava, 2005).

Martial and Methods

To achieve this work some material and methods were used and included S/W and H/W sides, in H/W side the materials included:

Specific mobile device (3G or LTE) was used to access application and web services

Private local network (intranet) was designed.

In S/W were some methods and application are designed and developed as follow:

Many E-services and applications were designed and developed that undertaken e-gov.

The environment of Zope server was used.

Plone and python language were used.

LDAP scheme was designed based on Linux Debian.

The WiMax technology as media was base.

S/W and H/W interactive interfaces were designed and used.

The framework of open source operating system was based.

By using the above material and methods we provide the ability to access the applications and services that were available in local servers that will agree with "ANY TIME ANY WHERE", so the added value of our work to support people which are live courtyard (rural and remote areas) . at fwrthermore in the practical side we design a prototype of Mportal and MSC (mobile switching center) to prove our concept.

Implementation Techniques of Mobile Government

According to Lu Jinjun, Shao Xijun. (Andersen, 2008), technologies that support the implementation of m-

government can be mainly classified into four groups:

Those based on wireless two-way radio-communication or broadcast;

Mobile voice services, SMS, WAP, GPRS, UMTS based on cellular phones;

Those based on mobile devices, including lap-tops, flat computers, PDA, pager, blue-tooth technology, RFID and GPS;

Those based on network Wi-Fi or WAPI wireless local area network (WLAN).

M-Government Features

The followings were some of the attractive features that prompt shift towards m-Government: in developing countries (Nkosi, 2010)

Number of mobile users and increasing penetration: more people than ever have ownership of mobile devices capable of accessing e-services and e-contents.

Mobiles connecting people to the Internet: In Ghana, urban users were using mobiles to receive an "Internet experience" through Wireless Application Protocol (WAP) services provided over General Packet Radio Service (GPRS).

Mobility: enables people to access content wherever they were.

Inclusiveness and Remote area

access: Mobile phones, can reach those areas where the infrastructure necessary for Internet services or wired phone services is difficult to setup. In the developing countries mobile government applications may become a key method for reaching citizens in far and wide areas and promoting exchange of communications.

Low Cost: mobile phones were a relatively low cost technology, which the common people can afford to have it as compared to Internet technology.

Ease of Learning: Usage of mobile devices was fairly simple thus making it easy for any common person to use it and to access information.

Easy Infrastructure Setup: Due to the simple architecture of mobile telephony, new mobile phone networks can be easily installed in countries where infrastructure was an issue and less economic constraint.

Improvement on e-Government effort: M-government was not a replacement to e-Government but complementary to it. Also, it helps in expanding the scope of e-Governance in the areas like e- Democracy, e- Participation, e-Voting and many other forms of communication between the citizen and the government (Coursey, 2008).

Democracy, e-Participation, e-Voting and many other forms of communication between the citizen and the government (Coursey, 2008).

M-Government Services

As stated m-Government exists to apply for four main dimensions in the public sector as illustrated in below (Andersen, 2006).

M-Communication: Providing information to the public was not a trivial activity. It was the foundation of citizen empowerment. Without relevant information citizens were unable to form intelligent opinions and, thereby, were unable to act on the issues before them meaningfully

M-Services: Providing a channel of communication between citizens and government via SMS, and enable G2C transactions as well. Some examples of existing m-Services include m-Parking, m-Teacher: m-library and crisis communication.

m-Democracy: m-Voting and the use of SMS and mobile devices for citizen input to political decision making is an m-Government application with tremendous potential to enhance democratic participation.

M-Administration

Integration E-Government and M-Government

E-government services and technologies have a rapid growth. Utilizing the innovative ITs, especially web-based applications, used to improve the basic and primary activity of governments and extending the related activities to the e-government. Nowadays, the process of development the mobile technologies and seamless technologies have created a new direction in e-government which called m-government (Coursey, 2008). Although e-government is transit to m-government, m-government is in its first stage of implementation and it has implemented completely in nowhere. Different factors such as technical infrastructure, information infrastructure, mobile telephone penetration rate, social conditions, security situations, and political decisions should be considered for transition from e-government to m-government (Garcia, 2005). M-government can be an enabler for e-government to simplify the service delivery to citizens through different tools. Also m-government is the use of mobile and wireless communication technology in government for service and information delivery to citizens and organizations; e-government service improvement is the goal of the m-government (Nava, 2005). E-government and m-government are not

two separated subjects, but m-government is a better choice for general information and services presentation to the citizens because in m-government, accessing to the information and services in any time and any place is possible through connected wireless tools to the internet (Coursey, 2008).

The cooperation of m-government and e-government is important especially for countries that have not heavy investment on e-government implementation. Nowadays, m-government is unavoidable. Influence of wireless tools and wireless network enable the developing countries to activate the employees of governments more through preparing the real time and up to date information. In addition, m-government increases the interaction of citizens with governments. Newfound services as location-based services, services that are related to the location of users, are motivation for m-government which increase the value added of presented services (Alijerban, 2010).

Results and Discussion

There is not a comprehensive methodology for m-government implementation. It is obvious that it is better to present some services of government through e-government infrastructure, but the presented methodology in this paper is adequate for services that are designed for government to citizen (G2C) relations for delivering the public services. So no well-defined methodologies available on how to implement government services to the different parties from present e-Government facility to future m-Government one. This methodology will be used to implement the delivery of services to citizens. This methodology, with little modifications placed in the different steps, can be applied for the

delivery of services to other parties like businesses, etc.

Mobile E-Government Services

The Term m-service extends the concept of web services to the wireless environment. It refers to requesting and running web services on wireless devices.

An application component is considered as an *m-service* if it is transportable through wireless networks; flexible in terms of composition with other m-services; adaptable according to wireless devices' computing characteristics; and accessible by wireless devices via a micro browser as a mobile web application or able to interact with a mobile client software component that consumes web services. As shown in the Fig. (1).

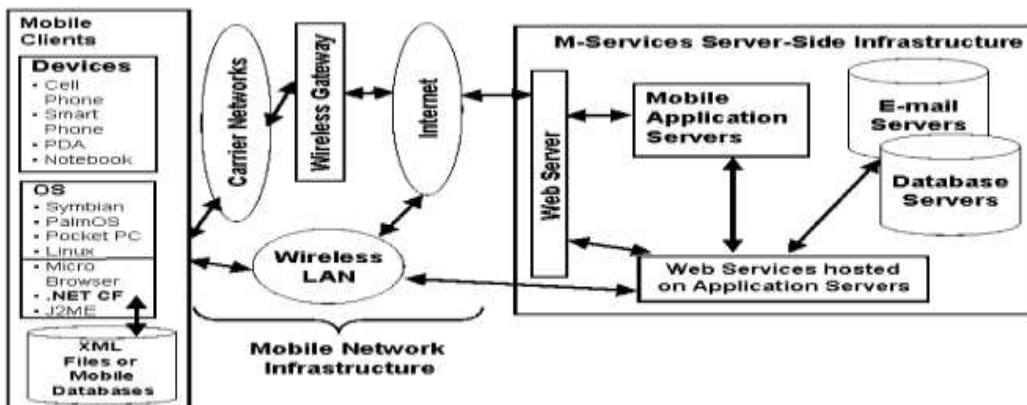
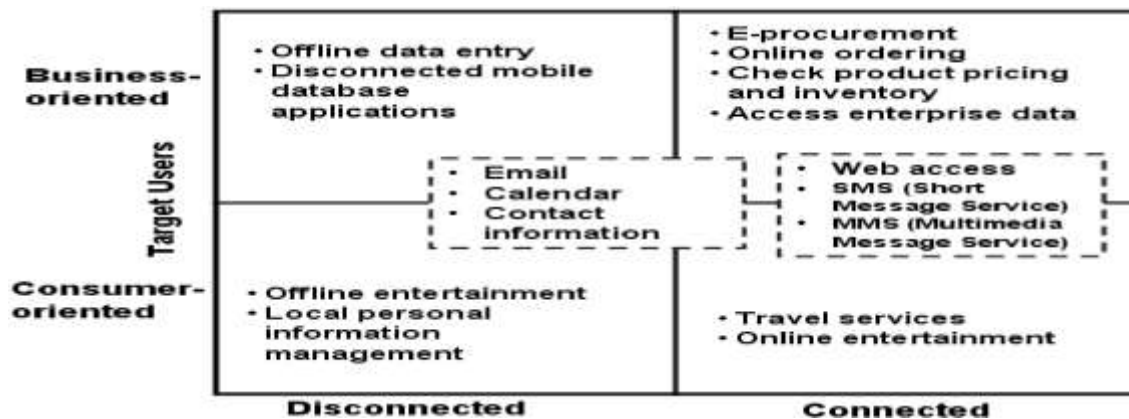


Fig. (1) Show layout of mobile network of E-Govnet

Classification of M-service

M-services include services that can be consumed in either connected or disconnected mode by consumers or business applications. Fig. (2) presents a matrix that classifies *m-services* two dimensions: target users (consumers vs. business) and network connection (disconnected vs. connected).



Disconnected applications can run in an offline mode. Data entered in the offline mode will be transferred and synchronized with the centrally stored data when mobile devices are connected to the network later on. E-mail service, calendar function, and contact information management serve as basic building blocks to *m-services* from all four quadrants in Fig. (2). For example, e-mail is an essential function in a mobile environment because it is often used in the context of business workflows in support of mission-critical enterprise applications. Web access, SMS, and MMS are basic services that

help deliver other value-added *m-services* in the connected mode. Business-oriented *m-services* in the connected mode include e-procurement, online price checking, ordering, shipping status tracking, and so on. These *m-services* can be used to integrate mobile applications with legacy systems or ERP systems.

Fig.(2) A classification of m-service

MPORTAL Gateway to Applications and services

The term *portal* was used to refer to well-known Internet search and navigation sites that provided a starting point for web consumers to explore and access information on the World Wide Web. The original portals were search engines. The initial value proposition was to offer a full text index of document content and a chance to take advantage of the hyper linking capabilities built into the web protocols.

Proof of concept (GovNet Network)

Government network (GovNet) is a part of E-government project which is deal with government employees and Government information , which is consist of Datacenter and network infrastructure (WiMAX)(*intranet network with controlling access to internet*) .The GovNet supports Government sector by exchange information (G2G). Layout infrastructure. As show in Fig. (3)



Fig. (3) Block Diagram of Mobile GovNet

Architecture of M-Service Portal

A web portal is an aggregation of heterogeneous web resources at a website to provide easy access to these resources. We propose an *m-service* portal architecture, as shown in Fig. (4), which integrates *m-services* to provide adaptive and personalized services and to accommodate the constraints of mobile devices.

An *m-service* portal can be either consumer-oriented or business-oriented. The architecture of the proposed *m service* portal consists of three major components:

List manager maintains a personalized list of pre-configured *m-services* (e.g., frequently-used hyperlinks to various *m-services*) specified by mobile users.

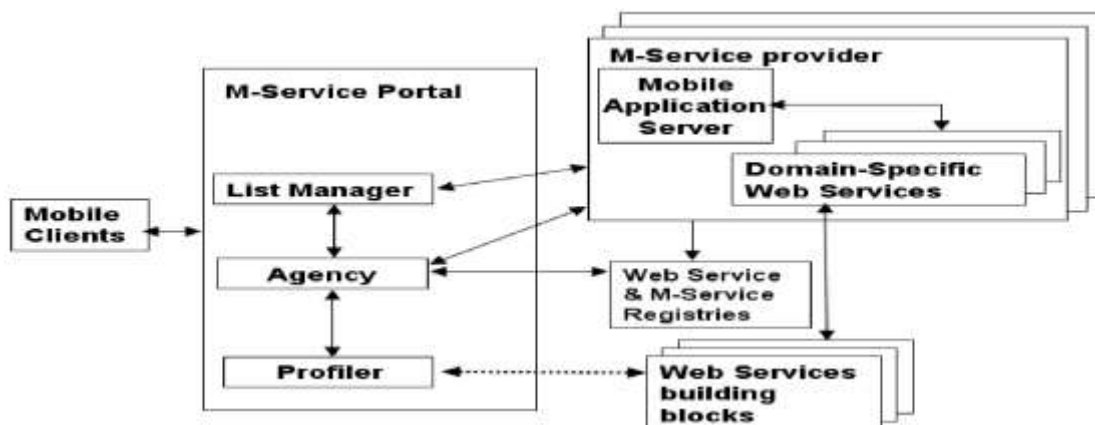


Fig.(4) An M-service portal Architecture

The list can be updated based on mobile users' access patterns by assigning higher scores to the most recently visited sites. It aims to reduce unnecessary data entry and search. The user can also use the List Manager to link to other m-service portals such as:

- Google Wireless Web Search. It allows users to search not only the 'Mobile web' created specifically for mobile devices, but also the entire World Wide Web.

- MSN Mobile. It provides mobile internet services similar to MSN services to users of mobile devices. Those services include e-mail, weather information, sports, news, personalized MSN alerts, as well as MSN Messenger.

Profiler is responsible for storing personal information and preferences such as financial profiles, health and insurance profiles, information needs (such as scores of sports games and local weather), message delivery preference for consumer-oriented m-services, and properties of mobile devices that users have (for customized content presentation). Business rules can be integrated into business-oriented

m-services such as e-procurement.

The management of profiles and preferences can be implemented using web services built upon external web service building blocks, so that the profiles and preferences can be easily shared with other m-service applications outside this m-service portal.

Agency uses intelligent agent technologies to reduce unnecessary interaction between m-services and the mobile user. Based on users' information recorded in the Profiler, agents can proactively collect relevant services and information on behalf of users.

Mportal of GovNet

The suggested Mportal of GovNet that can access by mobile device to connections to local and wide area government networks, and, public and private partnerships to extend Internet access in rural and remote areas. Mportal implementation involving the utilization of all kinds of wireless and mobile technology, services, applications and devices for improving benefits to the parties involved in e-government units Fig.(5) and Fig.(6) show Mportal of GovNet M-service list



Fig. (5) MPortal Govnet M-service



Fig. (6) Horde Email

Suggested M-Government

In the following steps we explain the interactivity between the mobile device (used by customer) and the *Mportal* to access the m-services those are available on the special intranet.

Step 1 : select the required mobile device to access the intranet(Nokia or Samsung) or any device can be used to interactive with wireless that have features of Wimax, Wi-Fi technology as shown in Fig.(7).



Fig. (7) Main Interface of Mobile Device

Step 2: now connect to access point by determine a specific Network (Govnet). The specific network select here is hotspot (dig-soc) as shown in Fig. (8).



Fig. (8) Access Point Page

Step 3: The connection between the mobile device and the special local host network was established as shown in Fig. (9).



Fig.(9) show login menu

Step 4: Determine the login to the selected network, where the security level is depending on the login and password as shown in Fig. (10).



Fig.(10) Entering Authorization Information

Step 5: In this step there are two facilities to accesses the network services, the first through the specific intranet (m-service or our m-portal) the second through wide web world (internet) where the customer can be accessed the available resources, as explained in the Fig (11). Now the customer can be accessed and used the available m-services (horde mail, human resource application etc.) as explained in the Fig. (12).



Fig.(11) access to internet



**Fig. (12) a. Access to mPortal
b. Access to application**

Suggestions and Recommendations

Mobile e-government is an important information channel to improve efficiency of urban government and social administrative functions, raise its capacity to serve the public and strengthen government's emergency handling ability. In order to enable mobile e-government to give strong support for governmental work, we give the following recommendations for the construction and development of mobile e-government system.

Establish mobile e-government laws and regulations. Improve laws and regulations concerning mobile e-government construction as soon as possible, so that standards of public services can be raised.

Carefully accomplish the overall planning and top-storey design of mobile e-government.

In its development, mobile e-government should not abandon the achievements of constructing original governmental information and e-government. Viewed from the growing trend of mobile e-government research, the following problems are worth discussion and research:

Restructuring of governmental services. How we can provide a good environment for the development of mobile e-government through clarification, definition and allocation of services of government departments.

Recreation of governmental processes. In the promotion process of mobile e-government, information technology is the basic method and tool in reconstructing governmental processes.

Resource pooling. First, resource sharing among various functional departments at the same level; second, resource sharing among governments at different levels; third, resource sharing between national power bodies and functional departments of the government; fourth, resource sharing between the government and the public of enterprises.

Service model of the government. A kind of small-scale new governmental organizational form with definite functions and boundaries can be ultimately realized through service restructuring, process recreation and resources pooling. Construction of mobile e-government is a gradual and long-term process, and the government should learn from experiences and lessons of other cities and developed countries and make full use of mobile communication technology to create a highly efficient, citizen-centered and service-oriented government.

Reference

Alijeban and M. Saghafi, F. (2010). "M-government Maturity Model with Technological Approach ",4th International Conference on New Trends in Information Science and Service Science Pages: 164-169 Provider: IEEE Publisher: IEEE

Andersen and H.Z. Henriksen. (2006). "E-government Maturity Models: Extension of the Layne and Lee model," *Government Information Quarterly*, vol. 23, no. 1, pp. 236-248.

Al Thunibat A. and Zin N.A.M. (2010). " Mobile Government Services in Malaysia: Challenges and Opportunities", International Symposium on Information Technology ISSN: 2155897 Volume: 3 Pages: 1244-1249 Provider: IEEE

Coursey and Norris D.F. .(2008). "Models of E-Government: Are They Correct? - An Empirical Assessment," *Public Administration Review*, vol. 68, no. 3, pp. 523-536.

Garcia and T.A. Pardo .(2005). "E-government Success Factors: Mapping Practical Tools to Theoretical Foundations". Proc. Proceedings of the International Conference on Mobile Business (ICMB'05), IEEE Computer Society.

Nava and I.L. Dvila .(2005). "M-Government for Digital Cities: Value Added Public Services," Proc. The Proceedings of the First European Mobile Government Conference, UK.

Nkosi, M. and Mekuria F .(2010). " Mobile Government for Improved Public Service Provision in South Africa", Pages: 733-737 Provider: IEEE.

Shahkoo and A. Abdullah .(2007). "A Strategy-based Model for E-government Planning", Proc. The Second

International MultiConference on Computing in the Global Information Technology.

Zarei.(2008). "Toward National E-government Development Models for Developing Countries: A Nine-stage Model," *The International Information and Library Review*, vol. 40, pp. 199-20

Comparison Ionospheric Critical Frequency ($foF2$) Measurements with IRI-2007 and IRI-2012 Model Predictions at Mid Latitude Station during Low and High Solar Activity

Saadiyah Hasan Halos Fahmi Abdul Rahman Mohammed

Ministry of Science and Technology/ Directorate of Space and Communications-
Atmosphere and Space Science Center

Baghdad- Iraq

E-mail: sadia_alhassan@yahoo.com

Abstract

Measurements of the critical frequencies, $foF2$, obtained from ionosonde DPS-4 at a mid latitude station in Rome (geographic coordinates 41.8°N, 12.5°E), Italy, have been compared with the International Reference Ionosphere (IRI-2007), (IRI-2012) models using Comite' Consultatif International Des Radio Communications (CCIR) and Union Radio-Scientific Internationale (URSI) coefficients, during low and high solar activity. The data coverage hourly seasonal values of $foF2$ for low and high solar activity years 2008 and 2012. By comparing the results of IRI models and measured values of $foF2$ at Rome, it was found that (1) generally, the $foF2$ obtained from the (URSI and CCIR Coefficients) for both IRI models are closely follow observed $foF2$ values. (2) In low solar activity year 2008, both IRI-2007 and IRI-2012 (CCIR and URSI Coefficients) give $foF2$ values close to the ones measured at Rome. (3) In high solar activity year 2012, the results of IRI-2012 give $foF2$ values with smaller range of deviation than IRI-2007 results from measured values. The comparative study gives feedback for new improvements of IRI-2012 model.

Keywords: Comparison, Critical Frequencies, Predictions and Solar Activity.

مقارنة قياسات الترددات الحرجة ($foF2$) لمحطة ايونوسفيرية عند خطوط العرض الوسطى مع تنبؤات الموديلات IRI-2007 و IRI-2012 خلال النشاط الشمسي الواطيء والعالي

سعدية حسن هلوس فهمي عبد الرحمن محمد

وزارة العلوم والتكنولوجيا/ دائرة الفضاء والاتصالات - مركز علوم الجو والفضاء

بغداد- العراق

الخلاصة

قورنت قياسات الترددات الحرجة لطبقة $F2$ ($foF2$) لجهاز الايونوسوند (DPS-4) في محطة روما (41.8°N, 12.5°E) في ايطاليا، مع تنبؤات موديلات المرجعية العالمية للايونوسفير للعام 2007 (IRI-2007) وللعام 2012 (IRI-2012) بأستخدام المعاملات المعتمدة من قبل اللجنة الاستشارية العالمية للراديو (CCIR) و الاتحاد الدولي لعلوم الراديو (URSI) خلال النشاط الشمسي الواطيء والعالي . تشمل البيانات المستخدمة قيم $foF2$ الساعية الفصلية عند النشاط الشمسي الواطيء في سنة 2008 و عند النشاط الشمسي العالي في سنة 2012. وجد عند مقارنة نتائج موديلات IRI و قيم $foF2$ المقاسة عند محطة روما، ما يلي: (1) بصورة عامة ، تتبع قيم $foF2$ المستخرجة من معاملات CCIR و URSI لموديلي IRI نفس نمط قيم $foF2$ المقاسة من جهاز الايونوسوند . (2) تعطي معاملات CCIR و URSI لموديلي IRI قيم $foF2$ مقاربة الى قيم $foF2$ المقاسة عند النشاط الشمسي الواطيء في سنة 2008. (3) تكون قيم $foF2$ المستخرجة من موديل IRI-2012 بمدى انحراف عن القيم المقاسة اقل من مدى انحرافها من موديل IRI-2007 عند النشاط الشمسي العالي في سنة 2012. دراسة المقارنة اعطت خلفية عن تحسينات جديدة لموديل IRI-2012.

الكلمات المفتاحية : مقارنة، الترددات الحرجة، تنبؤات و النشاط الشمسي.

Introduction

The International Reference Ionosphere (IRI), global empirical model of the ionosphere, is a widely used. IRI is based on experimental measurements of the ionospheric plasma by using space and ground measurements.

IRI describes monthly averages of the critical frequencies of the F_2 -layer in the current ionospheric altitude range of 50–1500 km. IRI predictions are most accurate in Northern mid-latitudes, because of the generally high station density in this part of the globe. Both of these regions have rather sparse ionosonde coverage, partly because of the harsh climate conditions, and as a result the IRI predictions are less accurate at equatorial and auroral latitudes.

One of the most important data sources for the IRI critical frequencies of the F_2 -layer is the worldwide network of ionosonde stations that has monitored the ionosphere with varying station density since the nineteen-thirties. Besides the ionosonde network, other data sources for the model development include the incoherent scatter (IS) radars, several compilations of rocket measurements, and satellite data from in situ and topside sounder instruments. The IS radars measure all of the IRI parameters over the full altitude range, but only a few radars are in operation worldwide. Their data are essential for the description of variations with time, season, and solar activity, whereas the satellite data are a primary source for the description of the global morphology of ionospheric parameters. Two different computer programs have been used as sub-routines by IRI: one is called the Comité Consultatif International Des Radio communications (CCIR Coefficient), which was developed by CCIR committee (CCIR, 1967), (CCIR, 1991) and the other is the Union Radio-Scientifique Internationale (URSI Coefficient), which was developed by

URSI Committee (Rush, *et al.*, 1983), (Rush, *et al.*, 1984), (Rush, *et al.*, 1989), (Fox, *et al.*, 1988).

A large number of papers deal with the comparisons between observed ionospheric data and the IRI model predictions:

The validation of IRI-2007 ionospheric model predictions over the Tehran area during a low solar activity period using data of ionospheric station of the Institute of Geophysics, University of Tehran, have been studied, and it is found that the best agreement occurs during the Summer and Winter, and the largest differences are observed in the Spring and Autumn (Ghader, *et al.*, 2011).

It is found that from comparison of ionospheric F_2 peak parameters foF_2 and hmF_2 with IRI2001 at Hainan, a better agreement between observations and IRI predictions with URSI coefficients in Summer and at low solar activity (Wang, *et al.*, 2009), and the same agreement is founded from comparison of neural network technique with IRI-2001 model ionospheric predictions during great geomagnetic storms for a mid-latitude station (Adewale, *et al.*, 2010). Also at Grahams town, South Africa, it is found from comparison between observed ionospheric foF_2 and IRI-2001 predictions over periods of severe geomagnetic activities, that the model generates good results with observed foF_2 values during geomagnetic storms (Adewale, *et al.*, 2010). Comparative study for foF_2 measurements with IRI-2007 model predictions during extended solar minimum, have been studied, and it is found that IRI provides reliable results that compare well with actual measurements was made (Zakharenkova, *et al.*, 2013).

The purpose of this study is to test the reliability of IRI-2012(the Newest Version of the IRI Model) and the oldest version IRI-2007. In this study, monthly hourly average of foF_2 obtained from IRI-2007 and IRI-

2012(CCIR and URSI Coefficients) during 2008 and 2012 are compared with observed values from mid-latitude station in Rome (Lat. 42° N, Long. 13° E). IRI-2012 is expected to give results more accurate to observed measurements than IRI-2007.

Materials and Methods

The University of Massachusetts Lowell's Center for Atmospheric Research (UMLCAR) has produced digisonde sounders, the Digisonde Portable Sounder(DPS-4), capable of making measurements of the ionosphere and providing real-time on-site processing and analysis to characterize radio signal propagation to support communications or surveillance operations. These DPS-4 distributed in many different regions in the world. Italy interested in monitoring and observing the ionosphere, therefore it has many of ionospheric sounders.

In this paper, measurements of hourly $foF2$ values obtained from Rome (DPS-4) during low and high solar activity years 2008 and 2012 were available in the Space Weather Prediction Center at National Oceanic and Atmospheric Administration (NOAA) at web site: http://www.swpc.noaa.gov/ftpmenu/list/siono_month.html.

The monthly hourly medians of $foF2$ were derived from IRI-2007 (CCIR, URSI) & IRI-2012 (CCIR, URSI) models for years 2008 and 2012 were downloaded from the IRI web sites at: http://omniweb.gsfc.nasa.gov/vitmo/iri_vitmo.html. and http://omniweb.gsfc.nasa.gov/vitmo/iri-2012_vitmo.html. respectively, depending on 12-month smoothed values of the sunspot number (Rz12) which obtained from IPS Radio and Space Services at the web site: <http://www.ips.gov.au/Solar/1/6>. The monthly hourly averages of $foF2$ are derived from hourly $foF2$ data of Rome station and compared with the corresponding ones of IRI models

during low and high solar activity 2008 and 2012.

Statistical analysis was used to calculate standard deviation (SDV) for monthly averages of observed $foF2$ parameter according to equation (1):

$$SDV = \sqrt{\frac{\sum[foF2_{means} - \overline{foF2_{means}}]^2}{(n-1)}} \quad (1)$$

Where $foF2_{means}$ was $foF2$ from measurements, $\overline{foF2_{means}}$ was the average and (n) was the number of data (Kutiev, and Marinov, 2007). The relative difference $\Delta foF2$ (%) is defined as (Bertoni, F., *et al.*, 2006):

$$\Delta foF2(\%) = \left[\frac{(foF2_{IRI} - foF2_{means})}{foF2_{IRI}} \right] * 100 \quad (2)$$

Equation (2) was applied on monthly hourly averages of $foF2$ obtained from IRI-2007 and IRI-2012 models and Rome station measurements, where $foF2_{IRI} = foF2_{CCIR}$ for CCIR coefficient or $foF2_{IRI} = foF2_{URSI}$ for the URSI one.

Results and Discussions

This paper focus on comparison of IRI-2007 and IRI-2012 with ionosonde measurements at mid latitude station during low and high solar activity years 2008 and 2012. Figure (1) showed the monthly sunspot number and its 12-month smoothed number for solar cycle 24 started in January 2008 and expected to reach the peak in May 2013. Figure (1) iwas drawn depending on data obtained from the source (SWPC, 2013). Monthly smoothed sunspot number for years 2008 and 2012 is used as input parameter in IRI models to predict monthly hourly $foF2$ for years 2008 and 2012.

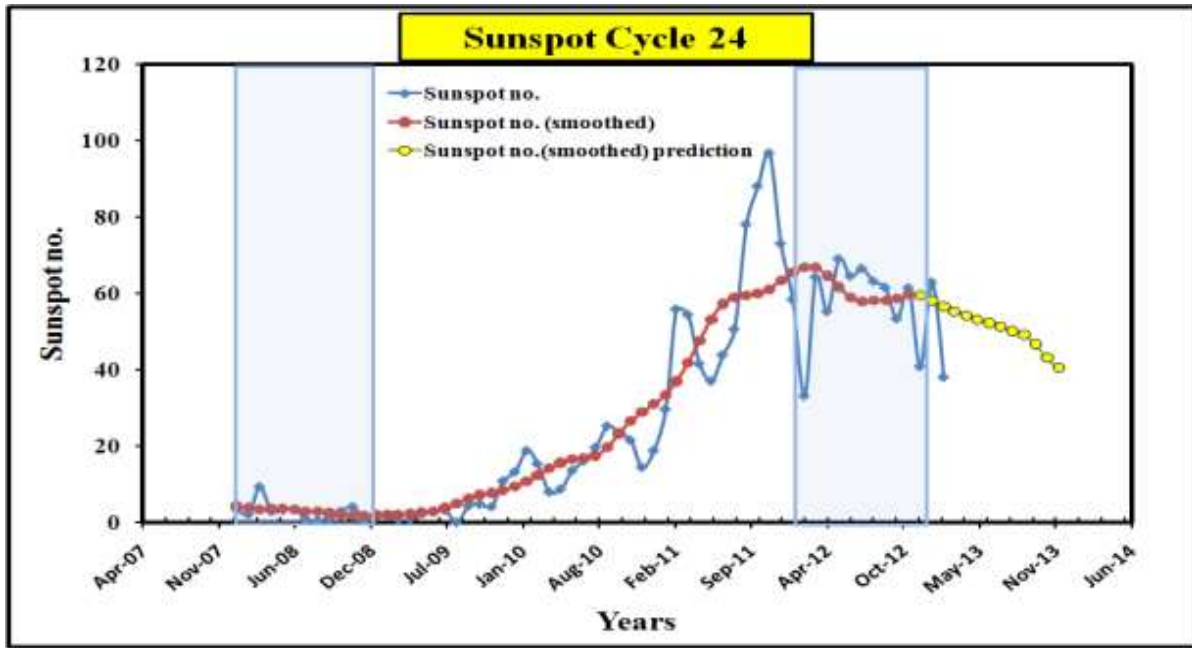
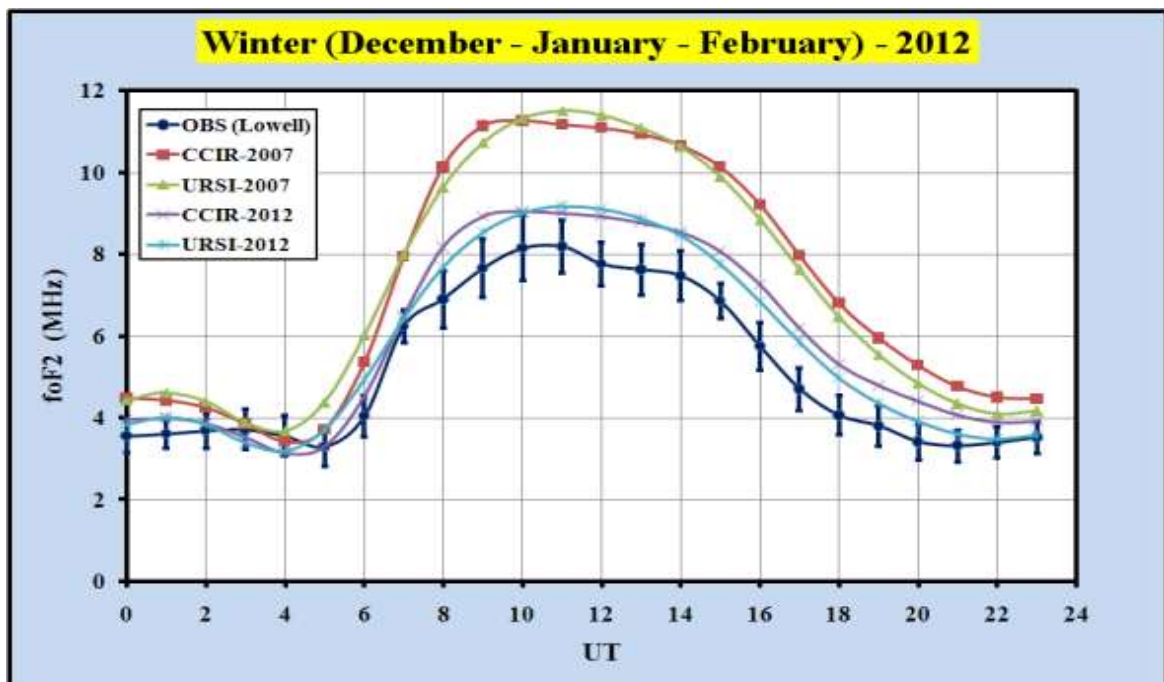


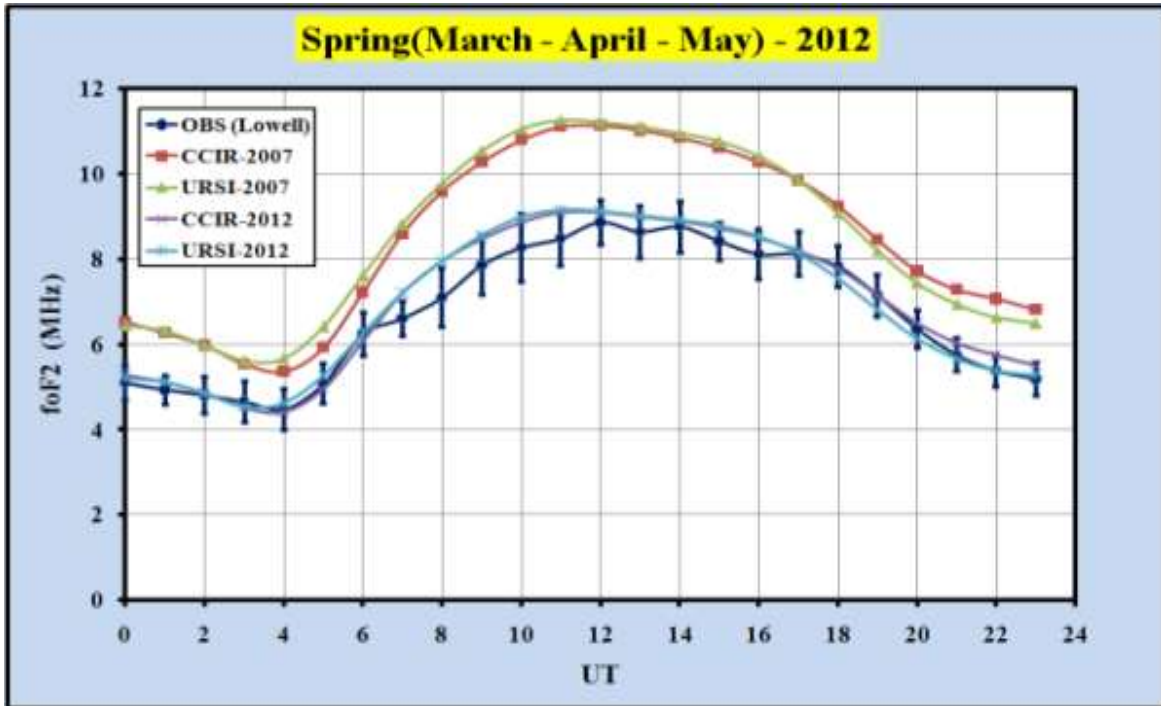
Figure (1) Sunspot Number with 12-Month Smoothed Number of Present Sunspot Number Cycle 24, Study Years are Shown in Shaded Columns.

Figure (2) shows the diurnal variations for different seasons of the observed $foF2$ values from Rome station and predicted IRI-2007 and IRI-2012 (using both the CCIR and URSI Coefficients) $foF2$ values.

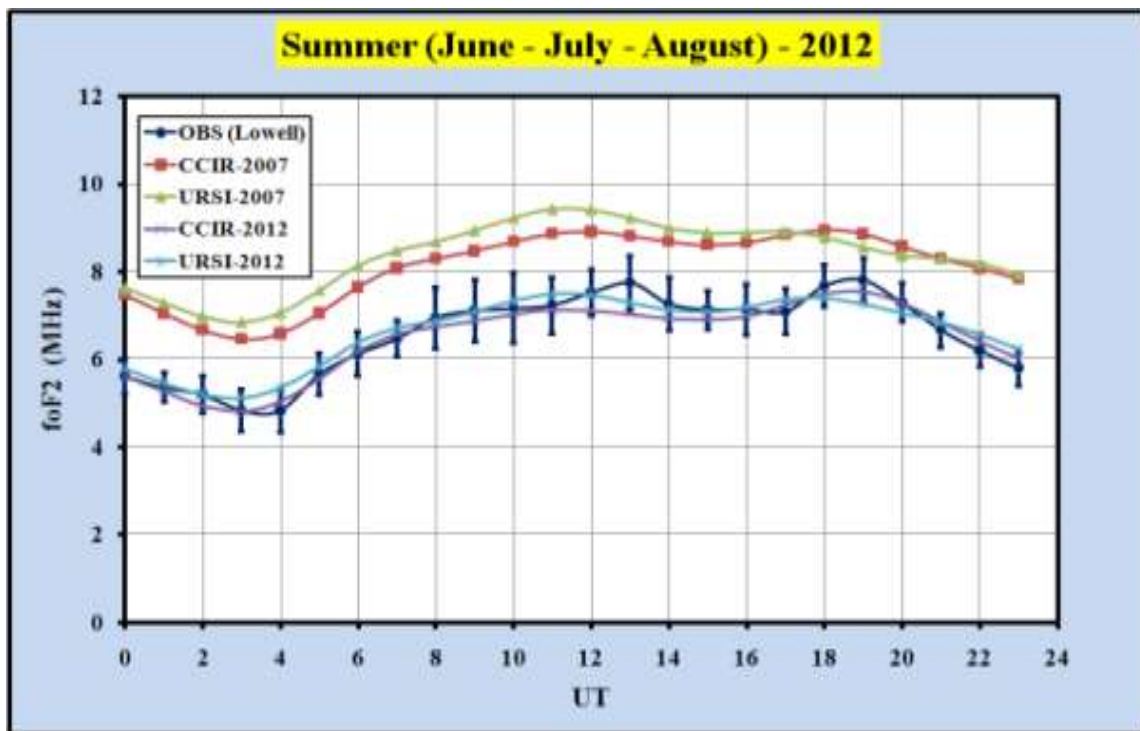
High solar Activity 2012



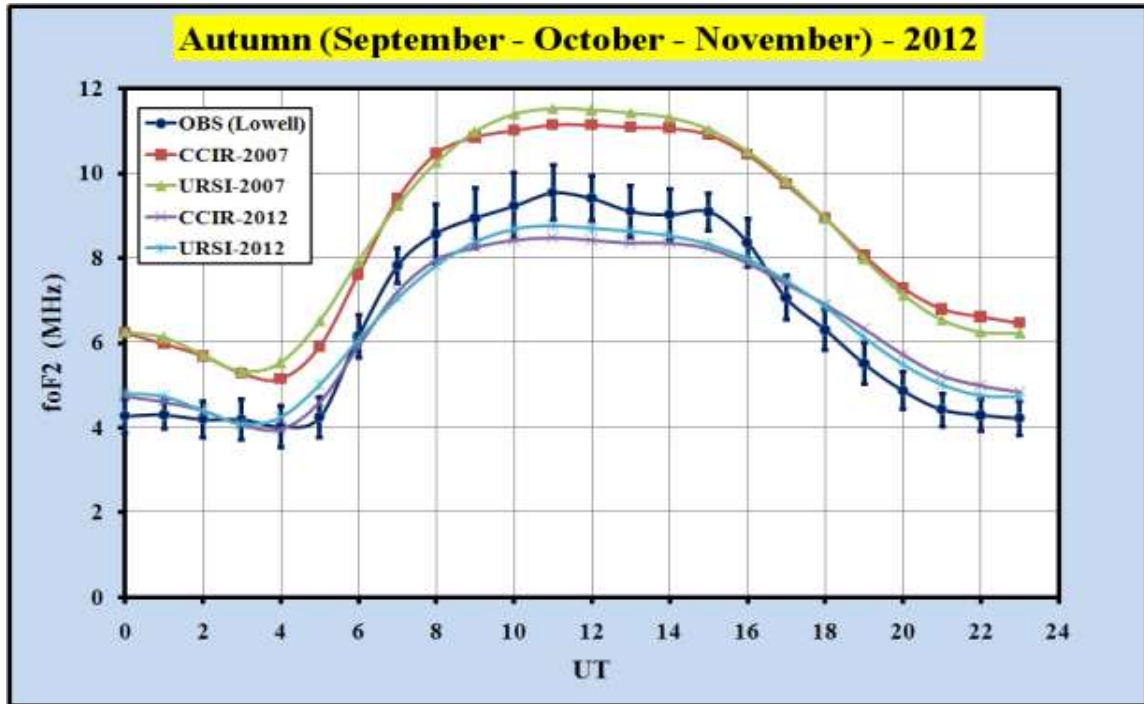
(a)



(b)



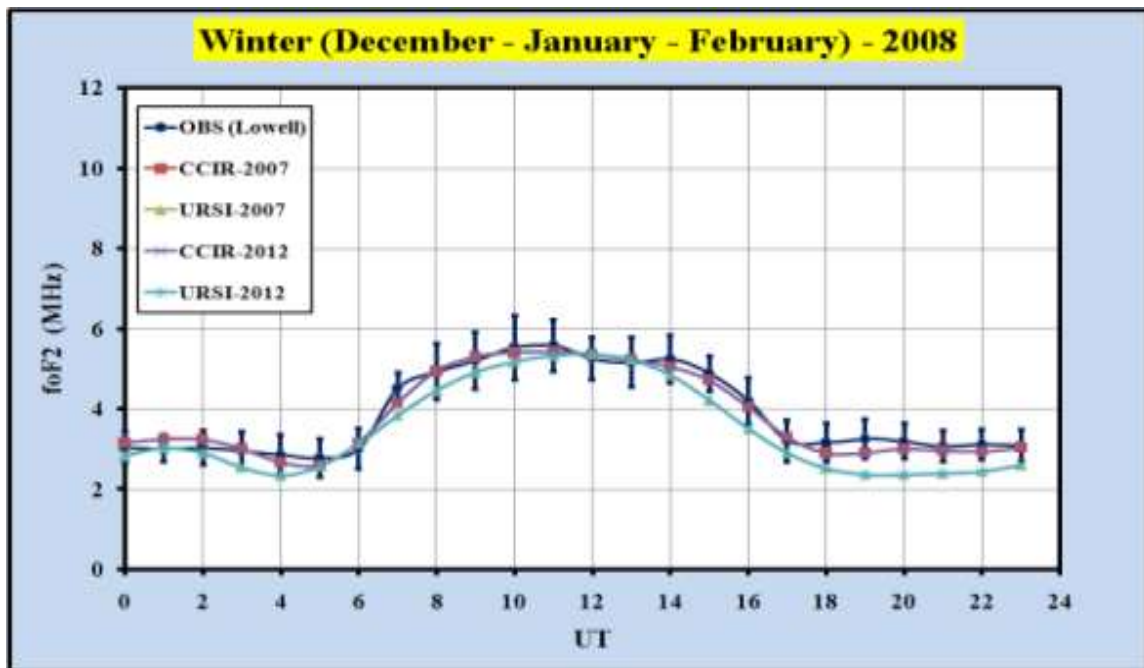
(c)



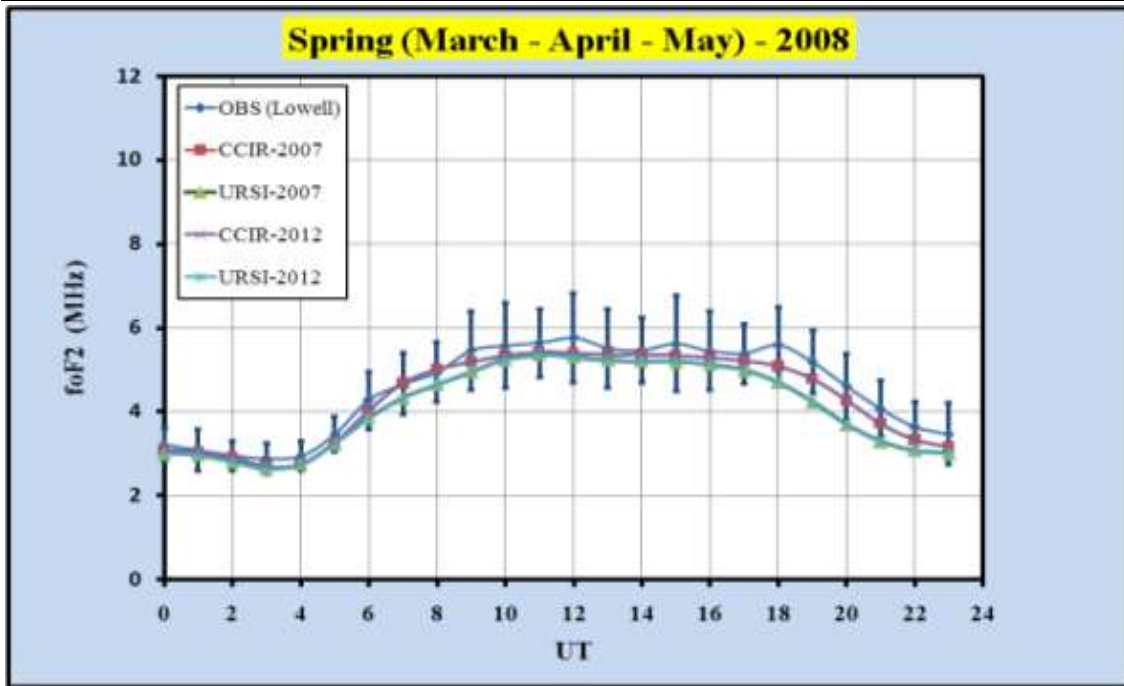
(d)

Figure (2) Plots of the Observed Diurnal *foF2* Variations with Standard Deviations for Different Seasons(a) Winter, (b) Spring, (c) Summer, and (d) Autumn in the Year 2012 at Rome Station with IRI-2007 and IRI-2012 Model Curves, using both URSI and CCIR Coefficients.

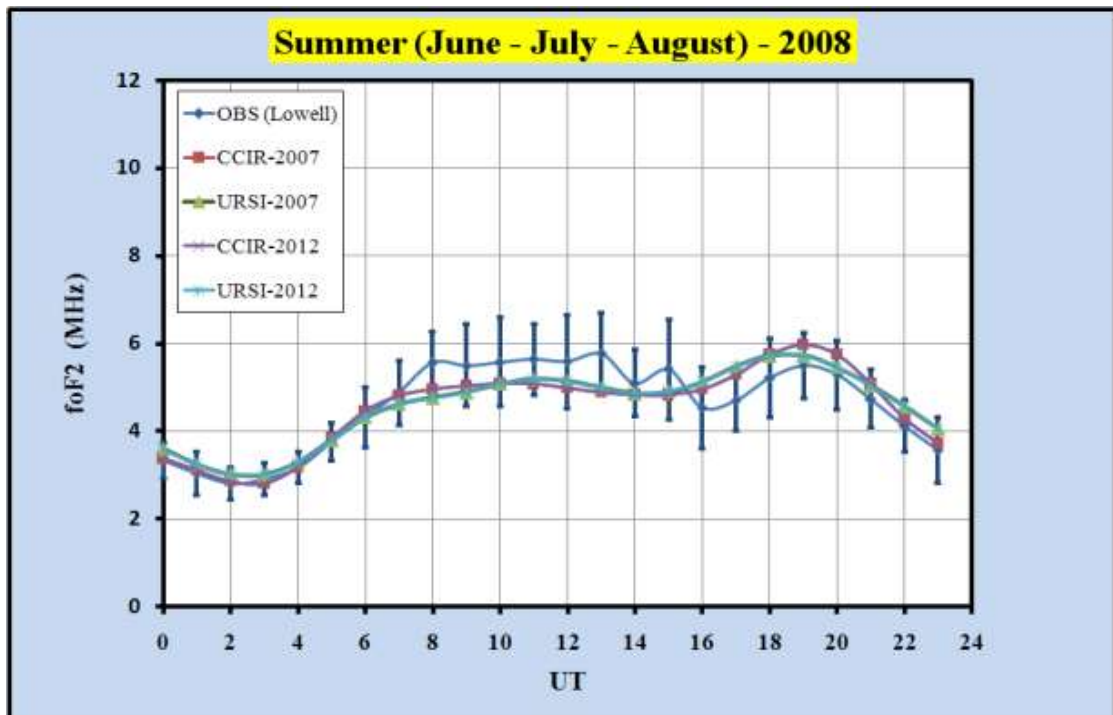
Low solar Activity 2008



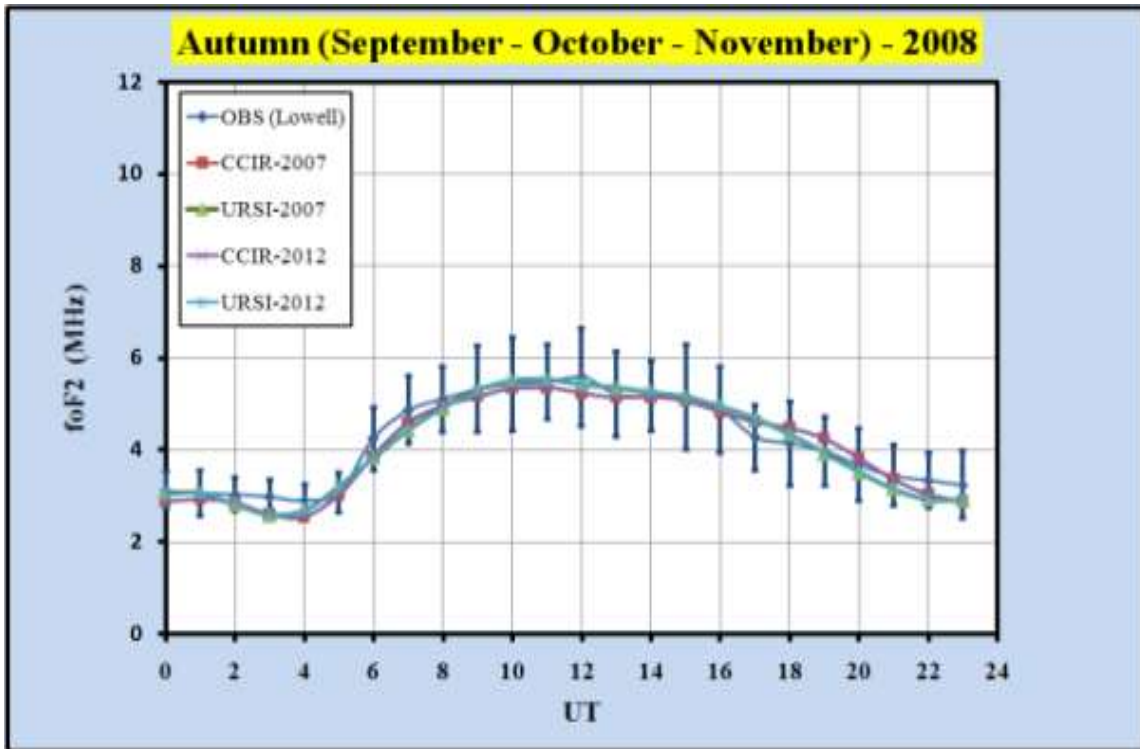
(a)



(b)



(c)



(d)

Figure (3) Plots of the Observed Diurnal $foF2$ Variations with Standard Deviations for Different Seasons (a) Winter, (b) Spring, (c) Summer, and (d) Autumn in the Year 2008 at Rome Station with IRI-2007 and IRI-2012 Model Curves, using both URSI and CCIR Coefficients.

Comparison is made for low and high solar activity years 2008 and 2012. The left four panels in figure (2) represent the diurnal average of $foF2$ with standard deviations for seasons of year 2012, while the right four panels in figure (3) for seasons of year 2008. It appears that is a good agreement between the observed $foF2$ and that given by IRI-2007 and IRI-2012 model predictions (CCIR and URSI Coefficients) for all seasons of year 2008. During Winter and Spring in 2012, observed $foF2$ values is underestimated the IRI-2007 and IRI-2012 models predictions, while observed $foF2$ values in Summer and Autumn in 2012 is underestimated the IRI-2007 model predictions and closed to IRI-2012 predictions.

Statistical analysis is applied by using relative difference $\Delta foF2\%$ between the observed $foF2$ values and that produced by IRI model (CCIR and URSI Coefficients) during low solar activity 2008 as shown in figure (4). It can be seen from figure 4(a), (b) that, $\Delta foF2\%$ between predicted values of $foF2$ from IRI-2007 and IRI-2012 using CCIR Coefficient and observed values, was high (IRI is overestimate observed $foF2$) especially at day hour (13 UT) in Summer, while URSI results in (c), (d) of figure (4) give a high $\Delta foF2\%$ at hours (4,16,17,18,19,20,21,22,23UT)in Winter season.

Figure (5) show $\Delta foF2\%$ between predicted values of $foF2$ from IRI-2007 and IRI-2012(CCIR and URSI Coefficients), and observed values during high solar activity year 2012.

Figure 5(a), (c) show that $\Delta foF2\%$ between IRI-2007 (CCIR and URSI Coefficients) and observed values, was high (IRI is overestimate observed $foF2$) at most of day hours and for all seasons, while $\Delta foF2\%$ between IRI-2012 (CCIR and URSI Coefficients) and observed values, was low (Observed $foF2$ is overestimate IRI) at

most of day hours and for all seasons, as shown in figure 5 (b), (d).

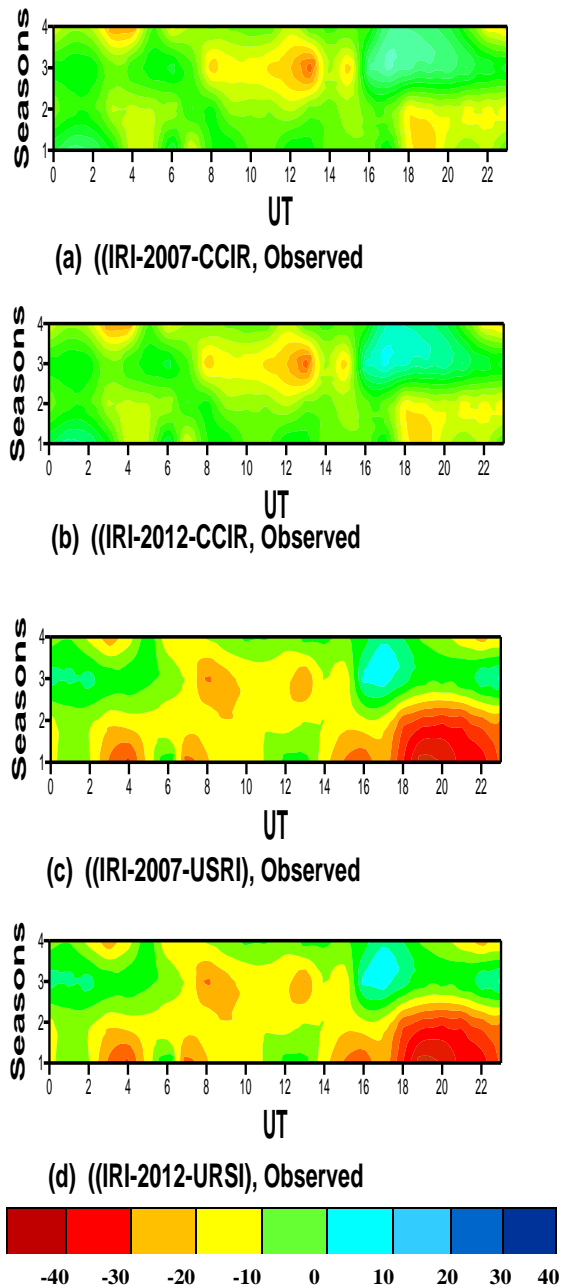


Figure (4) Contour Plots of the $\Delta foF2\%$ between (a) (IRI-2007-CCIR) and OBS, (b) (IRI-2012-CCIR) and OBS, (c) (IRI-2007-URSI) and OBS, (d) (IRI-2012-URSI) and OBS During Seasons: (1= Winter, 2= Spring, 3= Summer and 4= Autumn) of Low Solar Activity 2008.

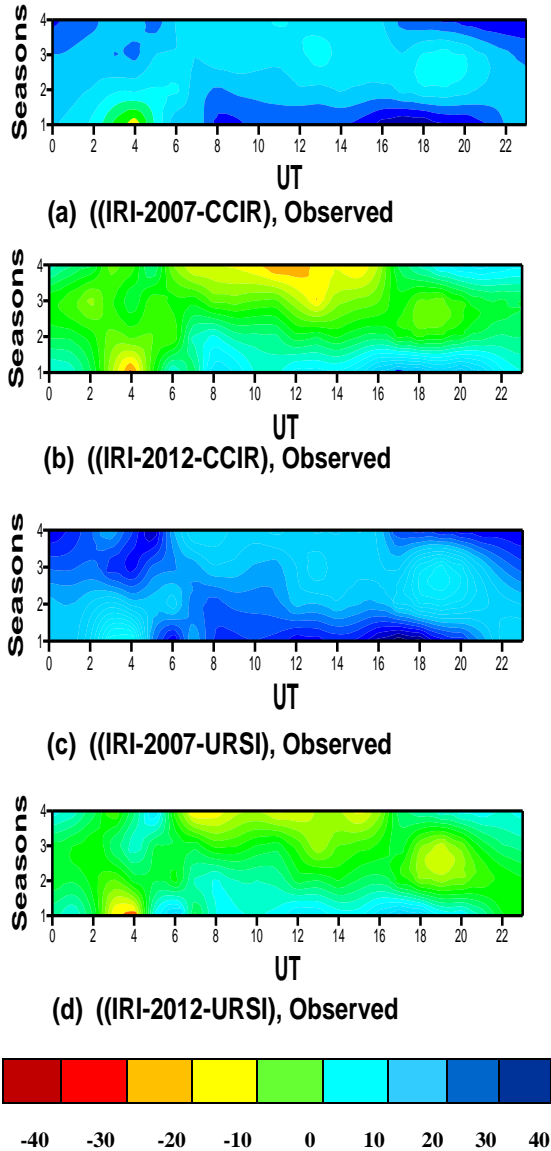


Figure (5) Contour Plots of the $\Delta foF2\%$ between (a) (IRI-2007-CCIR) and OBS, (b) (IRI-2012-CCIR) and OBS, (c) (IRI-2007-URSI) and OBS, (d) (IRI-2012-URSI) and OBS During Seasons (1=Winter, 2=Spring, 3=Summer, and 4=Autumn) of High Solar Activity 2012.

Table (1) Seasonal Day and Night Mean Relative Difference $\Delta foF2\%$ between the Predicted Values from IRI- 2007, IRI-2012 and Observed $foF2$ to the Observed Values for Rome During Low Solar Activity Year (2008).

Low Solar Activity (2008)								
Seasons	IRI-2007 CCIR		IRI-2007 URSI		IRI-2012 CCIR		IRI-2012 URSI	
	Day	Night	Day	Night	Day	Night	Day	Night
Winter	-8.9497	-2.1263	-8.9497	-18.452	-1.59	-2.113	-8.9357	-18.428
Spring	-3.9294	-6.4925	-8.1053	-12.834	-3.9156	-6.4731	-8.0901	-12.823
Summer	-4.5153	3.29728	-4.3698	5.86435	-4.5078	3.30173	-4.3547	5.87207
Autumn	-1.6692	-5.8585	-0.4855	-6.39	-1.6555	-5.8401	-0.4681	-6.3701

Table (2) Seasonal Day and Night Mean Relative Difference $\Delta foF2\%$ between the Predicted Values from IRI- 2007, IRI-2012 and Observed $foF2$ to Observed Values for Rome During High Solar Activity Year (2012).

High Solar Activity (2012)								
Seasons	IRI-2007 CCIR		IRI-2007 URSI		IRI-2012 CCIR		IRI-2012 URSI	
	Day	Night	Day	Night	Day	Night	Day	Night
Winter	31.13646	19.111	30.98354	18.92882	14.24161	8.17392	12.89147	4.354018
Spring	20.71521	19.27491	21.86163	18.64984	4.140115	2.009674	4.416146	0.213967
Summer	17.04095	21.66406	20.21919	23.3935	-2.58702	0.179643	0.283075	2.556574
Autumn	19.06135	29.71194	20.27777	30.05945	-6.37918	8.621061	-4.86969	8.87947

It can be seen from tables 1 and 2 that $\Delta foF2\%$ by using IRI-2007 and IRI- 2012 models, and observed $foF2$, in general, was low in low solar activity year 2008 and high in high solar activity year 2012. At day and night time, IRI-2012 by using both of CCIR and URSI Coefficients, $\Delta foF2\%$ was lower than the results from IRI-2007 for all seasons.

Conclusions

The results of the IRI-2007 and IRI-2012 models with the observations of critical frequencies $foF2$ conducted with the ionospheric sounder DPS-4 at Rome for low and high solar activity, have examined.

By analyzing the diurnal and seasonal averages of $foF2$ values for Rome in comparison with those predicted in the IRI-2007 and IRI-2012 models during low solar activity 2008 and high solar activity 2012, it was achieved that :

There is a very close similarity in the pattern of the daily variation of $foF2$ values for all seasons and for different solar activity.

In low solar activity 2008, both the CCIR and URSI Coefficients of the IRI-2007 and IRI-2012 models give $foF2$ values close to the ones measured.

In high solar activity 2012, the results of the IRI-2007 (CCIR and URSI Coefficients) are overestimated the measured values of $foF2$ for all seasons, but IRI-2012 model gives $foF2$ values close to the ones measured.

The CCIR results give more accurate predictions than the URSI results; because CCIR model is recommended over the continents (where Rome station location is over the continents and not over the ocean, so that the prediction results are more accurate by CCIR), while the URSI model is over the oceans.

Using a lot of years to make the results of seasonal mean relative difference $\Delta foF2$ % by using IRI-2007 model(CCIR Coefficient) are very close to its results by using IRI-2012 model(CCIR Coefficient) and the same with respect to (URSI Coefficient) for both day and night.

Acknowledgments

We would like to thank D. Bilitza at NASA/GSFC, Heliospheric Physics Lab. for his cooperation by giving the web site of the IRI-2012

References

Adewale, A.O.; Oyeyemi, E.O. and Ofuase, U.D. (2010) "Comparision between Observed Ionospheric $foF2$ and IRI-2001 Predictions Over Periods of Severe Geomagnetic Activities at Grahamstown, South Africa", *Advances in Space Research*, (45), Issue: 3, 368-373.

Adewale, A. O.; Oyeyemi, E. O. and Akala, A. O. (2010)" Comparison of Neural Network Technique with IRI-2001 Model Ionospheric Predictions During Great Geomagnetic Storms for a Mid-Latitude Station", *Journal of Sci. Res. Dev.*, (12), 75- 92.

Bertoni, F.; Sahai, Y.; Lima, W.L.C.; Fagundes, P.R.; Pillat, V.G.; Becker, F., and Abalde, J.R. (2006) "IRI-2001 Model Predictions Compared with Ionospheric Data Observed at Brazilian Low Latitude Stations", *Ann. Geophys.*, (24), 2191- 2200.

CCIR, (1967) "Atlas of Ionospheric Characteristics", Comit'ee Consultative International Des Radiocommunications, Report 340-4, Int.Telecommun. Union, Geneva.

CCIR, (1991) "Atlas of Ionospheric Characteristics", Comit'ee Consultatif International Des Radiocommunications, Report 340-6, Int.Telecommun. Union, Geneva.

Fox, M. W. and McNamara, L. F. (1988) "Improved World-Wide Maps of Monthly Median $foF2$ ", *J. Atmos. Terr. Phys.*, (50), 1077–1086.

Kutiev, I., and Marinov, P. (2007) "Topside Sounder Height and Transition Height Characteristics of the Ionosphere", *Adv. Space Res.*, (39), 759-766.

Rush, C.M.; Fox, M.; Bilitza, D.; Davies, K.; McNamara, L.; Stewart, F., and PoKempner, M. (1989) "Ionospheric Mapping: an Update of $foF2$

Coefficients”, Telecomm. J., (56), 179–182.

Rush, C. M.; PoKempner, M.; Anderson, D. N.; Stewart, F. G., and Perry, J. (1983) “Improving Ionospheric Maps Using Theoretically Derived Values of $foF2$ ”, Radio Sci. (18), 95–107.

Rush, C. M.; PoKempner, M.; Anderson, D. N.; Perry, J. C.; Stewart, F. G., and Reasoner, R. (1984) “Maps of $foF2$ Derived from Observations and Theoretical Data”, Radio Sci., (19), 1083–1097.

Sarmad, G.; Khalil, K. and Ahmad, R. (2011) “Validation of IRI-2007 Ionospheric Model Predictions over the Tehran Area During a Low Solar Activity Period Using Data of Ionospheric Station of the Institute of Geophysics, University of Tehran”, Iranian Journal of Geophysics, 5 (2), 16-27.

Space Weather Prediction Center, SWPC (2013) “Recent Solar Indices of Observed Monthly Mean Values”, NOAA.

<http://www.swpc.noaa.gov/ftplib/weekly/RecentIndices.txt>

Wang, X.; Shi, J.K.; Wang, G. J., and Gong, Y. (2009) “Comparison of Ionospheric $F2$ Peak Parameters $foF2$ and $hmF2$ with IRI-2001 at Hainan”, Advances in Space Research, (43), 1812–1820.

Zakharenkova, I.E.; Krankowski, A.; Bilitza, D. and Cherniak, Iu.V. (2013) “Comparative Study of $foF2$ Measurements with IRI-2007 Model Predictions During Extended Solar Minimum”, Advances in Space Research, (51), Issue: 4, 620-629.

Determination the Efficiency of Biological Treatment of Oil Pollutant by Gas Chromatography Technique

Sagida abass Hussain* Muna Mahmood Khudhair* Adel Saadi Salman**

Ministry of Science and Technology

* Directorate of Materials Research

** Environment and Water Research and Technology Directorate(EWRTD)

Baghdad-Iraq

E-mail: sagidaabass@yahoo.com

Abstract

Petroleum hydrocarbon especially in the form of crude oil has been a veritable source of economic growth to society from the point of view of its energy and industrial importance. For these reasons, the petroleum oil can cause environmental pollution during various stages of production, transportation and refining as well as spilling accident. Petroleum hydrocarbons pollution, ranging from soil, ground water to marine environmental, become an inevitable problem in the modern life. There are many various petroleum hydrocarbons clean-up technologies such as biological method, this method is efficient and economical compare with chemical and physical methods. The purpose of this study was to explore and study the efficiency of the fungi *Aspergillus Niger* which isolated from soil contaminated with crude oil in biodegradation of crude petroleum oil and using Gas chromatography technique to determine efficient of biological treatment. The results of this study show that the efficiency of fungi *Aspergillus Niger* to degrade petroleum oil hydrocarbon was 89% after 30 days of bioremediation treatment.

Key word: Biodegradation, Biological Treatment and Chromatography Technique

تحديد كفاءة المعالجة البيولوجية للملوثات النفطية باستخدام تقنية كروماتوغرافيا الغاز

ساجدة عباس حسين* منى محمود خضير* عادل سعدي سلمان**

وزارة العلوم والتكنولوجيا

* دائرة بحوث المواد/ ** دائرة تكنولوجيا معالجة البيئة والمياه

بغداد_العراق

الخلاصة

يعد وجود البترول مبدأ أساسيا من مبادئ النمو الاقتصادي ومصدرا مهما من مصادر الطاقة للعديد من الصناعات مما جعل منه واحدا من أهم الملوثات البيئية خلال عمليات الإنتاج والنقل والتكرير فضلا عن حوادث التسرب النفطية وشملت تأثيراته التربة والمياه والنظام البيئي مما دفع بالمهتمين بسلامة البيئة إلى استخدام العديد من التقنيات لإزالته، منها التقنيات البيولوجية التي تتميز بالكفاءة والفعالية وكونها طريقة اقتصادية بالمقارنة مع الطرق الكيميائية والفيزيائية. يهدف البحث إلى عزل فطر *Aspergillus niger* من التربة العراقية الملوثة بالنفط الخام واختبار كفاءته في إزالة النفط الخام فضلا عن استخدام تقنيات التحليل الكروماتوغرافي في تحديد كفاءة المعالجة البيولوجية. وبينت نتائج الدراسة كفاءة فطر *Aspergillus niger* في تفكيك الملوثات الهيدروكربونية النفطية ونسبة بلغت 89% بعد مرور 30 يوما على المعالجة البيولوجية.

الكلمات المفتاحية: التحلل البيولوجي، المعالجة البيولوجية و تقنية الكروماتوغرافي

Introduction

The increasing contamination of the environment by dangerous, toxic substances is a worldwide problem. Nowadays, routine and accidental spillages of petroleum derivative compounds are contaminating the air, soil, rivers, seas, and underground water (Vieira *et al.*, 2009). Petroleum hydrocarbons are one of the most frequently encountered pollutants in the environments habitats due to the increased usage of petroleum as the principle source of energy (Yu-Ying, 2011). Petroleum hydrocarbon especially in the form of crude petroleum-oil has been a veritable source of economic growth to society from the point of view of its energy and industrial importance. (Anthony and Okoh, 2006). There are many various petroleum hydrocarbons clean-up technologies. These can be categorized in three general schemes: chemical, physical and biological (Kermanshahi *et al.*, 2005). Bioremediation is believed to be one of the main processes used in the cleaning-up of contaminated soil and groundwater. This method is efficient and economical (Obire and Nwaubeta, 2001). The uptake of hydrocarbon by microorganisms is possible in three different mechanisms: hydrocarbon dissolved in the aqueous phase, direct cell contact and the uptake of hydrocarbon drops, and the uptake of pseudosolubilized hydrocarbon droplets by using biosurfactant (Bouchez *et al.* 1995; Kim *et al.*, 2002). It is known that the main microorganisms consuming petroleum hydrocarbons are bacteria and fungi as a method of biodegradation. Biodegradation using fungi have drawn little attention in the past two decades since most of the biodegradation researches focused mainly on the use of bacteria. Fungi produce enzyme that breakdown and degrade a wide range of recalcitrant pollutants such as polyaromatic hydrocarbons, chlorophenols, and

pesticides (Bumpus *et al.*, 1985). In addition, fungi have advantages over bacteria such as fungal hyphae that can penetrate contaminated soil to reach the PAHs that have spread beyond the top layer of the soil (April *et al.*, 2000). Besides, the fungi are capable to grow under environmental conditions of stress, for example: environment with low pH values or poor in nutrients and with low water activity. (Yateem *et al.*, 1998). Assessing the petroleum damage to environment and natural resources caused by accidental release of crude oil requires the design of appropriate and reliable chemical analytical methods for oil samples collected in the study area. The analytical data and results will provide essential information to document oil exposure pathways, to determine extent and degree of oiling, to evaluate the long term impact of spilled oil, to estimate recoverability of the injured resources, and to suggest effective clean-up strategies. Analytical methods and techniques for oil analysis have made major advances in recent years and the development continues. Gas chromatography (GC), mass spectrometry (MS), ultraviolet (UV), infrared spectroscopy (IR), fluorescence spectroscopy, supercritical fluid chromatography (SFC), and hyphenated techniques such as GC-MS, GC-FTIR, SFC-GC are used as techniques to evaluate oil analysis. Usually the biological method have been used such as turbidity, biomass and spectrophotometric to determine the efficiency the biological activity of removing petroleum pollutant which considered as not accurate in analysis.

The purpose of this work is to explore and study the efficiency of fungi in biodegradation of crude petroleum-oil by using the gas chromatography to determine type and amount of the hydrocarbon compounds which are presented in crude petroleum oil.

Material and Methods

Chemicals

Hexane, Chloroform, n-Pentane (all >99% purity) and Methylene Chloride (98% purity) were purchased from Fluka (Steinheim, Germany) and Methanol (99% purity) (analy gainland chemical company), Silica Gel (35-70 mesh ASTM) Merck. Crude petroleum oil was obtained from south of Iraq which had chemical composition as showed in the Table (1).

Table (1) Various Fractions of Crude Petroleum –Oil

Total Petroleum Hydrocarbons (TPH)			
Insoluble %	Soluble %		
Asphaltene	Alkane	Aromatic	NSO
12.2	58	17	12.8

Culture medium of Microorganism

The culture medium used throughout these studies consisted of: (1 g/L) Anhydrous Potassium Hydrogen Orthophosphate (K_2HPO_4); (1 g/L) Anhydrous Potassium Dihydrogen Orthophosphate (KH_2PO_4); (1g/L) Anhydrous Sodium Hydrogen Orthophosphate (Na_2HPO_4); (1g/L) Ammonium Nitrate (NH_4NO_3); (0.02g/L) Calcium Chloride 2-hydrate ($CaCl_2 \cdot 2H_2O$); (0.2g/L) Magnesium Sulfate ($MgSO_4 \cdot 7H_2O$); (0.05 g/L) of Iron Chloride ($FeCl_3$); (0.1%) Tween 80.

Experimental Procedure

Biodegradation method

The fungi *Aspergillus niger* which was used in the experiment was isolated from soil contaminated with crude petroleum-oil by following the reference (Griffin, 1972).

Replicates samples (n=3) were grown in 250ml Erlenmeyer flasks containing 100ml of culture medium. Then 1 gm of crude petroleum–oil was added to reach

a final concentration of 1 % (w/v). Three agar plugs ($1cm^2$) of the 24hr pure culture of *Aspergillus niger* were inoculated into the culture medium and then incubated at 37°C for 10, 20 and 30 days. Control tubes were prepared without the microorganism.

Chemical Analysis

Crude petroleum-oil was extracted from the mixture of *Aspergillus Niger* and culture medium by using sequentially extraction. In this extraction, 50ml of hexane followed 50ml of methylene chloride then 50ml of methanol: chloroform (1:1) were used, sequentially.

All of the three extracts were pooled and dried at room temperature by evaporation of the solvents under a gentle nitrogen stream in a fume hood. The dried-extract was dissolved in n-pentane (10ml) in order to separate it into soluble and insoluble (asphaltene) fractions. After that, the soluble fraction was evaporated in order to calculate the weight of residual (aliphatic, aromatic, and NOS compounds). In order to purify the residual, it was redissolve in n-pentane (10ml) and loaded on the top of a silica gel column (35-70 mesh) ($2cm \times 22cm$). After 5-10 mints a calculated volume of n-pentane (12ml) was added to receive the purified-residual. In order to use a calculated concentration, the purify residual was dried at room temperature and weighted. Then it was dissolved in appropriate solvent and injected into (GC) apparatus. The same procedure was repeated with the control tubes.

Chromatography(GC)

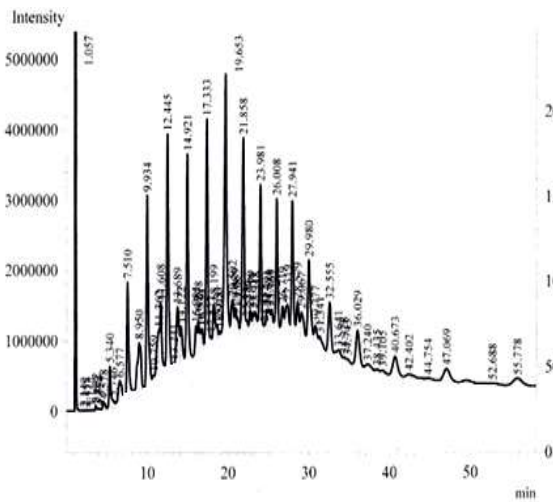
The fraction was analyzed by Gas Chromatography (GC) shimadzu, using a FID detector. The column was packed SE 30 (L3m, ID 2mm). The column temperature was 80-250 °C for 20min rate 5cc/min. The injector temperature was 260°C and detector temperature 270°C.

Results and Discussion

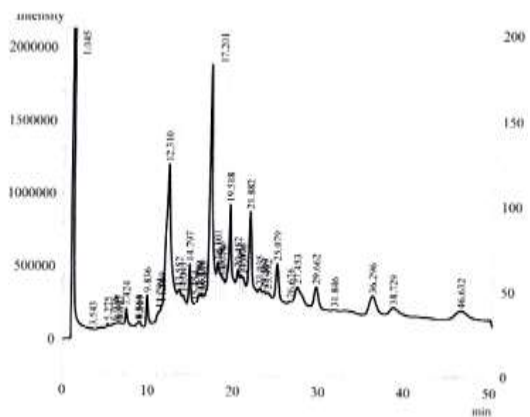
In this work, gas chromatography was used to evaluate the purified residue. Figure(1) shows the chromatograms of gas chromatography analysis of crude oil control(A), and purified residue after 10,20 and 30 days of biodegradation (B, C, and D).

In the period between 10-30 days, the biodegradation causes a dispersion of the oil, resulting a changes\

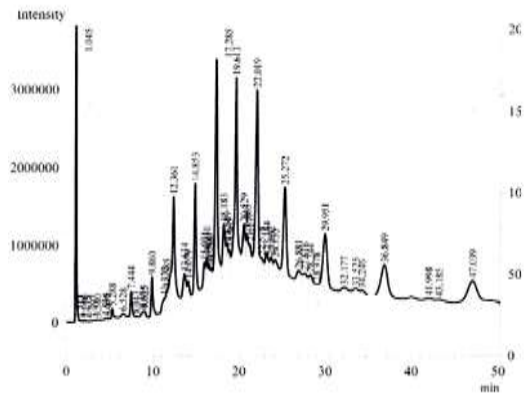
\ in the original feature of the crude petroleum-oil. It has been found that, a reduction of some hydrocarbon compounds and disappearance of others were occurred with increasing the biodegradation time.



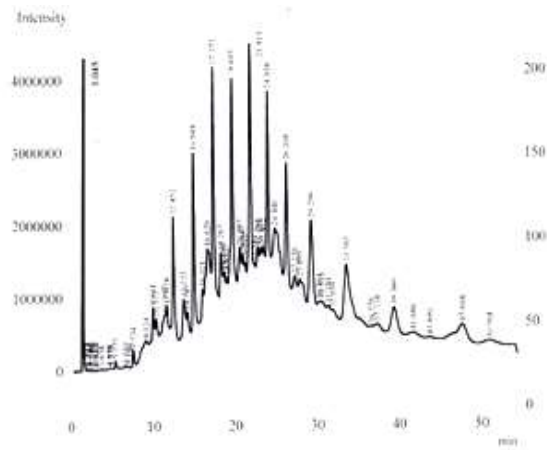
(A)



(B)



(C)



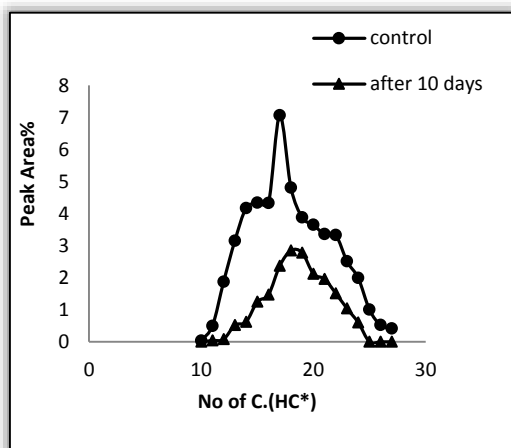
(D)

Figure(1) Gas Chromatographic Analysis of Crude Oil after Clean up. (A)Control and (B),(C),(D) after 10,20 and 30 Days Biodegradation Respectively

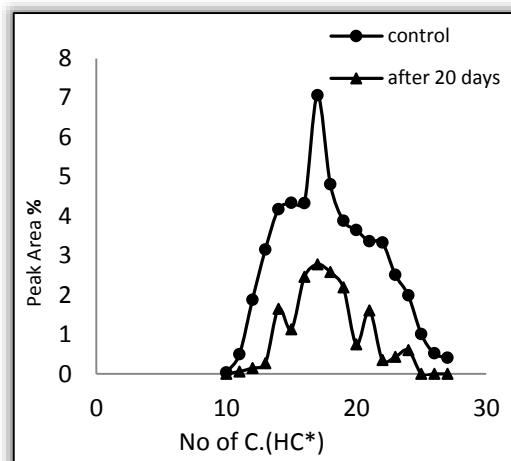
Related to the phenomena of disappearance of some hydrocarbons, it might be related that microorganisms can produce biosurfactants through biodegradation process. Microorganisms can survive and able to utilize the contaminant itself for growth on hydrocarbons that were insoluble in water. This surfactants enhance organic removal by raising the solubility of the hydrocarbons thereby making more of them available for degradation and facilitating transport of the hydrocarbons across the cell membrane of the

microorganisms (Khan, *et al.*2006). While the reduction of other hydrocarbons might be related to the petroleum oil as a complex mixture of aliphatic fraction, consisting of straight chain, branched chain , poly cyclic aromatic hydrocarbons, NSO and asphaltene fraction (Jain, *et al.* 2005), therefore a single microbial has only limited capacity to degrade all the fractions of hydrocarbons present, and the complex mixture of petroleum hydrocarbons might be influence each other's biodegradation the effects may go in negative as well as positive direction (Wackent. 1996).

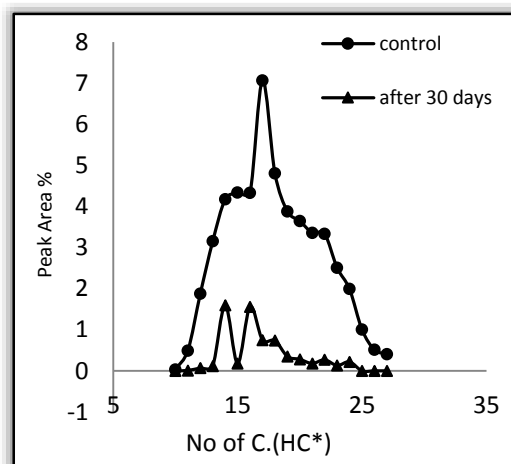
The degree of oil degradation was calculated in the total petroleum hydrocarbon degradation, by comparing the total area of the chromatograms containing *Aspergillus niger* with those of the controls (Xie *et al.*, 1999). Figure (1) shows the big changes in the crude composition. As expected, the biodegradation was occurred significantly. It was well documented that *Aspergillus niger* is able to degrade and resolved component of crude oil.



(A)



(B)



(C)

Figure(2) Comparison of Percentage of Peak Area between (HC*) and the Control (A, B, and C after 10,20 and 30 Days Biodegradation, Respectively)

Here in, HC* refers to n-paraffinic compounds (n-C10-C27), and HC** refers to isoparaffinic cycle, and aromatic compounds. The percentage of peak area was calculated by dividing the area of each individual peak on the total peak area of HC* or HC** in order to evaluate the biodegradation degree of *Aspergillus niger*.

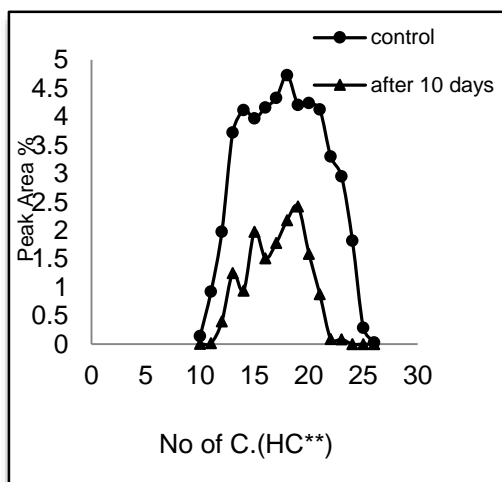
Figure(2) shows the relation between the percentage of peak area for normal paraffinic compounds(HC*) and the number of carbon atoms for both control and purified residue after 10, 20 and 30 days of biodegradation.

After 30 day, it is so clear that all the fractions (HC*) were completely utilized by *Aspergillus niger* except C14, C16, C17 and C18 which were suffered from drastic reduction.

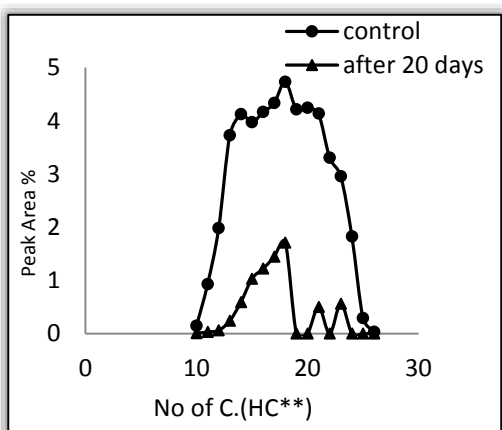
Figure (3) shows the relation between the percentage of peak area (C10-C11 and C11-C12....etc)((HC**) and the control after 10,20 and 30 days of biodegradation.

Comparison of the percentage of the peak area between (HC**) and the control after 30 days of biodegradation indicated that, all fractions of isoparaffinic and aromatic compounds are removal.

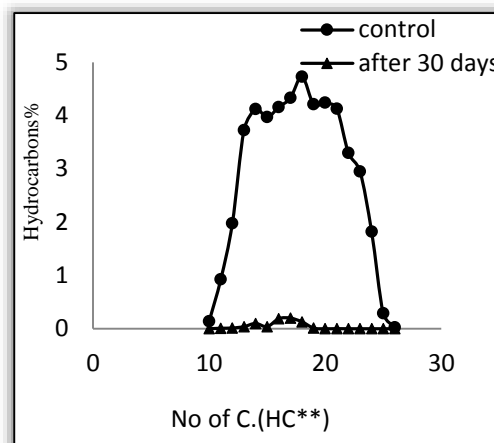
Figure (2) as compared with figure (3) indicated that, the degradation isoparaffinic and aromatic compounds are more than normal paraffinic.



(A)



(B)



(C)

Figure(3) Comparison of percentage of peak Area Between (HC**) and the Control (A, B, and C after 10,20 and 30 Days Biodegradation, Respectively)

Biodegradation using fungi have draw little attention in the past two decades since most of the biodegradation researchers focused mainly on the use of bacteria. Some reports indicate that the isolation of a pseudomonas strains degrade both aliphatic and aromatic fractions more than 90% after 21 days for two pseudomonas isolates (mixed culture) (Salam, *et al.*, 2011), while crude oil degradation rates of only 60 to 66% were reported by Adebusoye *et al.*, (2007) for pure culture strains isolated from polluted tropical streams after 20 days of incubation. In the present study, The results reported more than 89% degradation of crude oil by *Aspergillus niger* which were isolated from contaminated soil after 30 days of incubation.

The data presented in this paper was summarized in Table (2) which showed that the total biodegradation percentage of crude petroleum-oil after 10,20 and 30 days of biodegradation were 29,53 and 89%. after 10,20 and 30 days using the fallouing equation.

$$\text{Biodeg. \%} = \frac{\text{crude oil control} - \text{crude oil degraded}}{\text{crude oil control}} \times 100$$

Table(2) Biodegradation Percentage of Crude Petroleum Oil with Different Period Time

Period of Treatment	10days	20days	30days
Percentage of Biodegradation	29	53	89

Conclusions

Here in, fungi *Aspergillus niger* was isolated from the petroleum-contaminated soil in order to use this fungi to degrade the crude petroleum oil. It has been found that the efficiency of *Aspergillus niger* is time- dependent. The degradation rate increases with period of degradation to reach an efficiency of 89% after 30 days. The potential of GC to detect the oil fractions was used to determine the degradation efficiency of *Aspergillus niger*. At the same time, it has been noticed that isoparaffinic fractions and compounds (HC**) was reduced more than n-paraffinic compounds and fraction (HC*). Comparing with other works, our study calculates and compares both of (HC*) and (HC**) compounds and fractions while other works calculated for the crude petroleum –oil as one fraction. We believe that this work can add an advance step to the petroleum industry.

Recommendations

Using of some techniques which are more efficient such as GC-mass and HPLC in order to determine quantity and quality of lower concentrations for all oil's fractions, besides using other type of fungus or mixing more than one fungus for more degradation to oil's fractions.

Acknowledgment

Our thankful goes to Dr. Azhar Kamel for her contribution in writing this paper.

References

Adebusoye, S.A.; M.O. Ilori, O.O. Amund, O.D. Teniola and S.O. Iatope, 2007. Microbial Degradation of Petroleum in a Polluted Tropical Stream.

World J. Microbiol. Biotechnol., 23: 1149–1159

Anthony, I. and Okoh, (2006). Biodegradation Alternative in the Cleanup of Petroleum Hydrocarbon Pollutants. *Biotechnology and Molecular Biology Review* 1(2),38-50.

April, T.M.; Fought, J.M. and Currah, R.S. (2000). Hydrocarbon-degrading Filamentous Fungi Isolated from Flare Pit Soils in Northern and Western Canada. *Canada J. Microbiology* 46,38–49.

Bouchez, M.; Blanchet, D. and Vandecasteele, J.P. (1995). Substrate Availability in Phenanthrene Biodegradation: Transfer Mechanisms and Influence on Metabolism. *Appl. Microbiol. Biotechnol.* 43,952–960.

Bumpus, J.A.; Tien, M.; Wright, D. and Aust, S.D. (1985). Oxidation of Persistent Environmental Pollutants by a White Rot Fungus. *Science* 228,1434–1436.

Griffin, D.M.(1972). *Ecology of Soil Fungi*. Chapman and Hall. Landon.

Kermanshahi; Pour, A.; Karamanev, D. and Margaritis, A. (2005). Biodegradation of Petroleum Hydrocarbons in An Immobilized Cell Airlift Bioreactor. *Water Res.* 39,3704–3714.

Kim, I.S.; Fought, J.M. and Gray, M.R. (2002). Selective Transport and Accumulation of Alkanes by *Rhodococcus Erythropolis* S14 He. *Biotechnol. Bioeng.* 80,650-658.

Khan,K.; Naeem, M.; Javed Arshed, M., and Asif, M.(2006). Extraction and Characterization of Oil Degradation Bacteria. *Journal of Applied Sciences* 6(10): 2302-6

Salam, L.B.; Obayori, O.S.; Akashoro, O.S. and Okogie,G.O. (2011).

Biodegradation of Bonny Light Crude Oil by Bacteria Isolated from Contaminated Soil. *Intrnational Journal of Agriculture and Biology*. 13: 245-250.

Jain, R.K.; M. Kapur, S.; Labana, B.; Lal, P.M.; Sarma, D.; Bhattacharya and I.S. Thakur, (2005). Microbial Diversity: Application of Microorganisms for the Biodegradation of Xenobiotics. *Curr. Sci.*, 89: 101–112

Obire, O. and Nwaubeta, O. (2001). Biodegradation of Refined Petroleum Hydrocarbons in Soil. *J. Appl. Sci. Technol.* 5,43–46.

Vieira, P. A. ; Faria, S. ; Vieira, R. B. ; De Franc, F. P. and Cardoso, V. L. (2009). Statistical Analysis and Optimization of Nitrogen, Phosphorus and Inoculums Concentrations for the Biodegradation of Petroleum Hydrocarbons by Response Surface Methodology. *World J. Microbiol. Biotechnol.* 25,427–438.

Yateem, A.; Balba, M.T. and Al-Awadhi, N.(1998). "White Rot Fungi and Their Role in Remediating Oil-Contaminated Soil". *Environment International*, 24, 181-187

Yu-Ying Li, (2011). The Influences of Tween 60 and Rhamnolipid on the Bioremediation of n-hexadecane . *Restrictions apply*, 13,32-55.

Wackett, L.P. (1996). Co-metabolism: Is the Emperor Wearing Any Clothes? *Curr. Opin. Biotechn.* 7,321-325.

Xie, G.; Barcelona, M.J. and Fang, J. (1999). Quantification and Interpretation of Total Petroleum Hydrocarbons in Sediment Samples by a GC/MS Method and Comparison with EPA 418.1 and a Rapid Field Method. *Anal chem* 71; 1899-1904.

Efficacy of Electrical Resistivity Imaging Technique in Mapping Bedrock in Some Regions of South Iraq

Nadia Ahmed Aziz Zaidoon Taha Abdulrazzaq Hayder Abdul Zahrah Alwan
 Ministry of Science and Technology/ Space Directorate and Communication-
 Geophysics Researches Center
 Baghdad-Iraq
 E-mail: nadia_naa@yahoo.com

Abstract

Two-dimensional (2D) electrical resistivity imaging (ERI) method was used to detect the contact between sediment and bedrock some regions of south Iraq. ABEM Terrameter LS used for data collection, using three 2D electrical resistivity profiles. For the fieldwork, two-dimensional surveying carried out along three profiles using Dipole-dipole array with 8 m electrode spacing. The maximum depth of investigation was 50 m.

The data analyzed and explained 2D inversions by the RES2DINV software. The obtained data analyzed, and 2D models of the subsurface generated. The resistivity data were inverted into subsurface electrical sections using the least-squares inversion technique. Then, the contact between the bedrock and sediment was observed. Our results indicate well-defined boundary in the resistivity structure that can be used to estimate the quantity of sediments covering bedrock.

Keyword: Geo-electrical, Resistivity, 2D Inversion, Bedrock, and Subsurface Mapping.

كفاءة تقنية تصوير المقاومة الكهربائية في الطبقة الأساس في بعض مناطق جنوب العراق

نادية احمد عزيز زيدون طه عبد الرزاق حيدر عبد الزهرة علوان
 وزارة العلوم والتكنولوجيا/ دائرة الفضاء والاتصالات - مركز بحوث الجيوفيزياء
 بغداد-العراق

الخلاصة

استخدمت تقنية التصوير المقاومة الكهربائية ثنائي الأبعاد لتحديد الطبقة الأساس لبعض مناطق جنوب العراق باستخدام جهاز (ABEM Terrameter LS) لجمع البيانات وبطريقة Dipole-dipole لمسح المقاطع الطولية ثنائية الأبعاد وبمسافة 8 م بين قطب واخر وكان اقصى عمق للاختراق 50 متر. مسحت ثلاثة مقاطع طولية للمقاومة الكهربائية ثنائية الأبعاد.

حللت وفسرت البيانات ثنائية الأبعاد بواسطة برنامج RES2DINV لاعداد النموذج ثنائي الأبعاد لتحت الارض. استخدمت تقنية المربعات الصغرى لتفسير البيانات ولرسم الموديل النهائي وتفسيره ومن ثم حدد الحد الفاصل بين الرواسب والطبقة الصخرية الصلبة. اظهرت النتائج وجود حدود واضحة المعالم في قيم المقاومة والتي تم عن طريقها تحديد الحد الفاصل فضلاً عن تقدير كمية الرواسب الواقعة فوق الطبقة الصخرية الصلبة.

الكلمات المفتاحية: جيوكهربائية، المقاومة، عكس البيانات ثنائية البعد، الطبقة الأساس و رسم الخرائط التحت السطحية.

Introduction

Electrical resistivity techniques have been used to determine the location of various geologic and soil strata, bedrock fractures, faults, and voids. In the earlier applications, the technique was considered to be very labour intensive. The development of the 2D multi-electrode surveys has been able to reduce this aspect of the survey (Heather *et al.*, 1999).

Bedrock can be define as a solid rock that underlies loose material, such as soil, sand, clay, or gravel.

Many works have been done to establish a relationship between soil engineering test and ERI data (Israil and Pachauri, 2003; Cosenza *et al.*, 2006; Gay *et al.*, 2006). Another important advantage of ERI is that it produces continuous information of the subsurface and probes into several meters below the surface. Survey design and layout strategies that produce optimum information using different Electrical Resistivity Imaging (ERI) configurations and set up in different geological settings have been the topic of several studies (Alumbaugh and Newman, 1999; Stummer *et al.*, 2004; Ayolabi *et al.*, 2009).

2D electrical resistivity imaging survey is produced by injecting current into the ground through two current electrodes and measuring the resulting voltage difference at two potential electrodes. This process is repeated for many current/potential electrode configurations to produce a pseudo-section of apparent resistivity. The resultant data are then processed using a 2D inversion. Variations in the underlying sediment or rock units indicated by different electrical resistivities can then be observed as strong gradients in resistivity. Although the subsurface resistivity distribution could then be interpreted and mapped by eye, we will show that this subjective method should be done with caution because of the diffusive nature of the

electrical field. This paper aims at defining a better location of the electrical interface between a high-resistivity layer and a low-resistivity layer, like the bedrock–sediment contact (Marr and Hildreth, 1980; Vafidis *et al.*, 2005).

The most commonly used arrays in the 2D electrical imaging surveys are conventional arrays such as the Wenner, Schlumberger or dipole-dipole arrays. These arrays are often well understood in terms of their depths of investigations, lateral and vertical resolution and signal- to- noise ratios (Al Fouzan, 2008). The Dipole-dipole array gives good horizontal resolution, while the Wenner and Schlumberger arrays are more intended for vertical resolution. In the application to karst surveys, the dipole-dipole array has provided highest precision of ground changes sensitivity and has the greatest sensitivity to vertical resistivity boundaries (Zhou *et al.*, 2002).

The electrical profiles were interpreted using the RES2DINV resistivity software. This calculation program is based on the least-square method with an enforced smoothness constraint, modified with the quasi-Newton optimization technique. The inversion method constructs a model of the subsoil using rectangular prisms and determines the resistivity value for each of them, minimizing the differences between the observed and calculated apparent resistivity values (Loke and Barker, 1996; Loke and Dahlin, 2002).

The goal of the present work aimed to investigate the efficiency of 2D of electrical resistivity imaging technique in mapping bedrock.

Materials and Methods

Geology of the Studied Area

Dibdibba Formation (Pliocene-Pleistocene)

The formation consists of conglomeritic sandstone and claystone, intermddled by pebbly sandstone layers, occasionally contains vertebrate bones. These

beds overlain by pebbly calcareous sandstone partly micaceous.

The sandstone is whitish grey, massive. The conglomerate is composed of gravel size: sandstone, claystone fragments (in the lower part); detrital carbonate fragments, quartz and igneous rocks fragments.

Generally, the thickness increases southwards. The exposed thickness ranges from 2m to 9m.

The formation covered uncomfortably by Quaternary deposits such as sand sheet deposits and sand dune deposits (Hassan *et al.*, 2002).

Quaternary

The Quaternary sediment has a huge area extent covering. These sediments are of Pleistocene and Holocene ages and were deposited by fluvial, eolian and lacustrine agencies (Hassan *et al.*, 1989).

They were composed of various types of sediment which originated mostly by eolian and rain-wash processes; they were mixture of various fragments, clayey, silty and sandy, also with admixture of gravels, they were mostly calcareous, gypsums, sometimes compacted, friable and jointed with gypsum veins.

Study and Survey Design

Three profiles were measured namely line A, B and C. Dipole-dipole array was used for all profiles to get better depth penetration in the outer parts of the survey area. The electrode spacing was 8 meters.

A general 2D profile acquisition of the resistivity data was fairly straightforward. The data processed and inverted using RES2DINV software. The program generates the inverted

resistivity-depth image for each profile line.

Results and Discussion

Line A

The resistivity values for this line vary between 5 and 1101 ohm.m, the total length was 320 m, the depth of investigation 50 m, and the RMS was 2.5% after 5 iterations (Fig. 1).

The inversion resistivity image shows three different layers, the first layer contains quaternary deposits showing high resistivity that ranges from 518 to 1101 ohm.m. The resistivity values for the intermediate layer was 115 ohm.m, which may represent Debdibba Formation. The third layer shows low resistivity value (5-25 ohm.m) and was interpreted as an unconfined aquifer.

In this section, the separation between the sediment and the bedrock was appear at depth 6.2 m.

Electrical Resistivity technique proved to be versatile, fast in delineating aquifers and mapping shallow subsurface anomalies. It had a wide flexibility in covering large data with dense sampling for a given block of rock mass and at the same time intelligent in acquiring different strength of signals from the subsurface geological characteristics. The true resistivity models resulted from mathematical computation, standard and advanced inversion approaches in conjunction with the measured apparent resistivities had been helpful in resolving the geological formations, depth of bedrock, and the groundwater in different geological terrains with much more confidence and with high resolution as compared to conventional resistivity methods. The essence of this unique technique is seen and proved worth in the present day geo-scientific study.

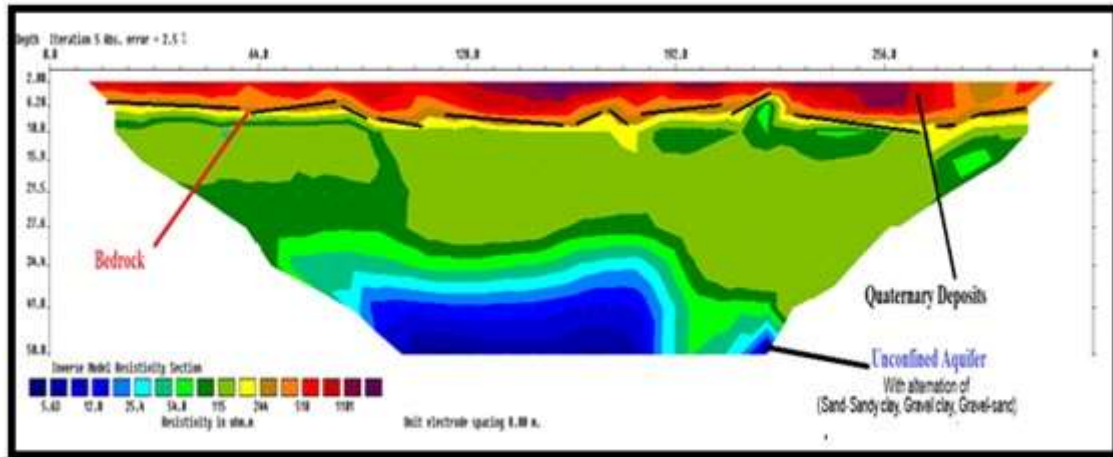


Fig. (1) Inverted Resistivity Section for Line A.

Line B

The inversion result of this line was shown in Figure 2. The resistivity values ranged between 3 and 953 ohm.m. The RMS 3.28 % after 5 iterations. The length of this spread line is 320 m with maximum depth of investigation 49.9 m. The surface uppermost layer showed relatively high resistivity values ranging from 424 to 953 ohm.m which it is quaternary deposits, with an inhomogeneous resistivity distribution which could be explained by the variable

water content levels within the same layer. To the lower, a low resistivity area (with green color) with a value 83 ohm.m may be interpreted as Debdibba Formation. The third layer shows low resistivity value 7 ohm.m and was interpreted as an unconfined aquifer. In this section, the separation between the sediment and the bedrock was appear at depth 7 m.

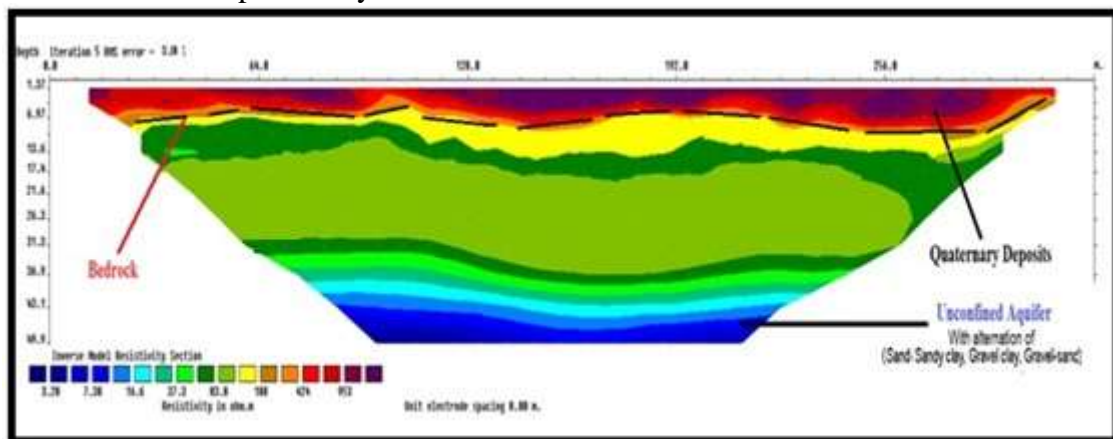


Fig. (2) Inverted Resistivity Section for Line B.

Line C

The 2D inversion resistivity pseudo-section of Line C (Fig. 3) trends from W to E direction, the total length of survey line was 320 m, and the maximum depth of investigation was 50 m. The resistivity values vary from 2 to 795 ohm.m with RMS 4.5% after 5 iteration.

In this section, the separation between the sediment and the bedrock was appear at depth 10 m.

The subsurface resistivity image along Line C appears basically identical to that obtained from Line A and Line B, with the same layers appeared.

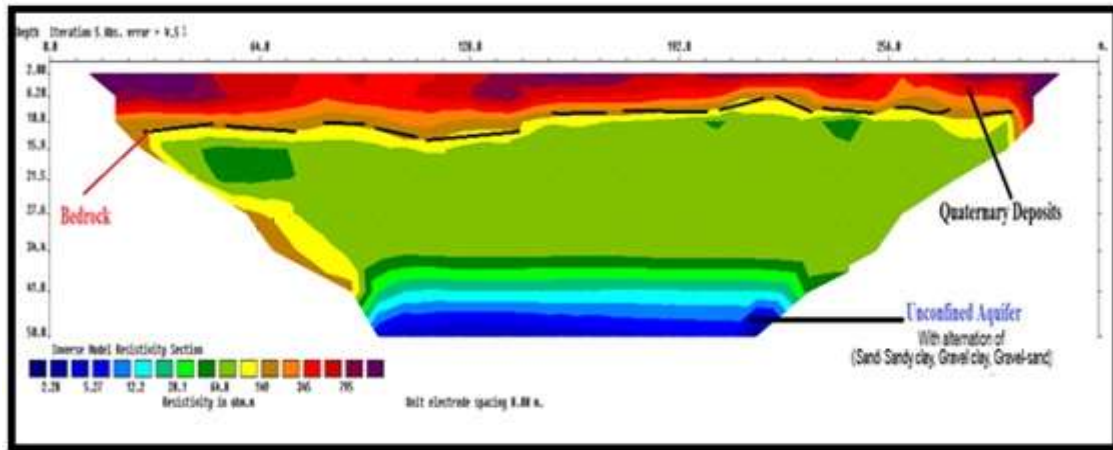


Fig. (3) Inverted Resistivity Section for Line C.

Conclusion

The results showed a consistent distribution in all 2D ERI profiles, where a shallow high resistivity zone (interpreted to be Quaternary deposits) covers a low-resistivity zone (interpreted to be bedrock). Apparently, resistivity of the sediment follows a log-normal distribution with an average of about 345 ohm.m. The broad distribution of resistivity in these sediments is likely influenced by randomness associated with grain size, pore space, and level of water saturation.

Electrical resistivity is non-destructive and can provide continuous measurements over a large range of scales. Besides, it is an attractive method for soil characterization in the contrary to regular drilling which perturbs the soil.

It is found that Dipole-dipole array is a suitable choice to be considered and used for such investigation as it is suitable for field conditions; provides high signal strength and provides adequate penetration depth.

The ability of geo-electrical imaging to indicate changes in rock conditions by means of varying resistivity makes it a valuable tool in the pre-investigation.

References

AL Fouzan, F.A. (2008) Optimization Strategies of Electrode Arrays Used in Numerical and Field 2D Resistivity

Imaging Surveys, PhD. thesis, Universiti Sains Malaysia, 25-48.

Alumbaugh, D.L. and Newman, G.A. (1999) Image Appraisal for 2-D and 3-D Electromagnetic Inversion, In: Proceedings of the Society of Exploration Geophysicists Annual Meeting, New Orleans, 1998. New Orleans, Louisiana, The Society of Exploration Geophysicists, 2–10.

Ayolabi, E.A.; Folorunso, A. F.; Adeoti, L.; Matthew, S. and Atakpo, E.(2009) 2-D and 3-D Electrical Resistivity Tomography and Its Implications, A Paper Presented at the 4th Annual Research Conference and Fair Held at the University of Lagos, Akoka, 8th Jan, 2009, p189. www.ivsl.org.

Cosenza, P.; Marmet, E.; Rejiba, Y.; Tabbagh A. and Charlery, Y. (2006) Correlations between Geotechnical and Electrical Data: A Case Study of Garchy In France, Journal of Applied Geophysics, 60, 165-178.

Gay, D. A.; Morgan, F. D.; Vichabian, Y.; Sogade, J. A.; Reppert, P. and Wharton, A. E. (2006) Investigations of Andesitic Volcanic Debris Terrains: Part 2 – Geotechnical, Geophysics, 71, B9–B15.

- Hassan, H.A.;** Ismail, S.K and Al Dabbas, M. (1989) Regional hydrogeological Condition of Dibdiba Basin Southern Iraq. J.Agric. Water Resal. Res, 8 (1),167-180.
- Hassan, K.M.;** Al-Khateeb, A.A.G.; Khlaif, H.O.; Kadhum, M.A. and Saeed, F.S. (2002) Detailed Geological Survey for Mineral Exploration in Karbala – Najaf Area. Part 1, Geology. GEOSURV, Int. Rep. 2874.
- Heather, L.;** Stahl, A.; Leberfinger, L. and Warren, J. (1999) Electrical Imaging: A Method for Identifying Potential Collapse and other Karst Features Near Roadways. Science Applications International Corporation, Middletown Pennsylvania, USA.
- Israil, M. and Pachauri, A.K.** (2003) Geophysical Characterization of a Land Slide Site in the Himalayan Foothill Region, Journal of Asian Earth Sciences, 22, 253-263.
- Kearey, P.;** Brooks, M.; and Hill, I. (2002) An Introduction to Geophysical Exploration, Blackwell Science, Oxford.
- Loke, M.H. (2012)** Tutorial: 2D and 3D Electrical Imaging. <http://www.georentals.co.uk/Lokenote.pdf>.
- Loke, M.H. and Barker, R.D.** (1996) Rapid Least-squares Inversion of Apparent Resistivity Pseudosections by
- Marr, D. and Hildreth, E.** (1980) Theory of Edge Detection. Proc. R. Soc. Lond., B 207, 187–217.
- Stummer, P.;** Maurer, H. and Green, A.G. (2004) Experimental Design: Electrical Resistivity Data Sets That Provide Optimum Subsurface Information, Geophysics, 69 (1), 120–139.
- U.S. Army Corps of Engineers** (1995) Engineer Manual 1110-1-1802, CECW-EG, Department of the Army, Washington, DC 20314-1000.
- Vafidis, A.;** Economou, N.; Ganiatsos, Y.; Manakou, M.; Poulioudis, G.; Sourlas, G.; Vrontaki, E.; Sarris, A.; Guy, M. and Kalpaxis, Th. (2005) Integrated Geophysical Studies At Ancient Itanos (Greece). J. Archaeol. Sci. 32, 1023–1036.
- Zhou, W.;** Beck, B.F. and Adams, A.L. (2002) Effective Electrode Array in Mapping Karst Hazards in Electrical Resistivity Tomography. Environmental Geology 42, 922–928.
- Loke, M.H. and barker , R.D. (1996) Raped Least – Squares Irver Sion of Apparent Resis tivity pseudosechons by a Quasi-Newton Method. Geophys Prospect 44,131–152.
- Loke, M.H. and Dahlin, T.** (2002) A comparison of the Gauss-Newton and Quasi-Newton Methods in Resistivity Imaging Inversion, Journal of Applied Geophysics, 49, 149–162.
- Milson, J.** (2003) Field Geophysics”, 3rd Edition, John Wiley and Sons Ltd, 232.

Structural and Optical Properties of Cadmium Selenide Thin Films Prepared via Direct Current Sputtering Technique

Baha'a A.M. Al-Hilli * Muhammed Khmas Khalaf ** Anwar Abd Alzahra Muhammed *

*Al-Mustansiriyah University /College of Education- Physics Dept.,

**Ministry of Science and Technology /Material Research Directorate- Applied Physics
Research Center,
Baghdad-Iraq
E-mail:bahahilli@yahoo.com

Abstract

The influence of preparation condition on the structural and optical properties of Cadmium Selenide (CdSe) thin films deposited onto glass substrates was studied. The structural investigations performed by means of X-ray diffraction (XRD) technique showed that the films have polycrystalline, hexagonal structure, Moreover, the AFM study showed that the film of uniform nano-grain size about 10nm. Transmission spectra in the spectral domain (200-1200nm), were investigated. The values of some important parameters of the studied films (absorption coefficient, optical energy band gap and refractive index) were determined from these spectra. The values of the energy gap, E_g (allowed direct transitions), calculated from the absorption spectra, ranged between 2 and 2.2eV.

Key words: Thin Film, CdSe, DC Sputter, and Optical Energy Band Gap.

الخواص التركيبية والبصرية لأغشية الكاديوم سيلينايد المحضرة بالترديد المستمر

بهاء عبد الرسول مجيد الحلي*، محمد خماس خلف**، أنوار عبد الزهرة محمد*

*الجامعة المستنصرية / كلية التربية- قسم الفيزياء

** وزارة العلوم والتكنولوجيا / دائرة بحوث المواد - مركز الفيزياء التطبيقية

بغداد - العراق

الخلاصة

درس في هذا البحث تأثير ظروف التحضير على الخواص التركيبية والبصرية لأغشية كاديوم سيلينايد المرسبة على قواعد زجاجية بطريقة الترديد. الخواص التركيبية لهذه الأغشية درست باستخدام فحوص حيود الأشعة السينية (XRD) والتي بينت أن هذه الأغشية لها تركيب متعدد التبلور وبالشكل السداس، وأظهرت نتائج مجهر القوة الذرية AFM أن الأغشية المحضرة ذات سطوح متجانسة وحجم حبيبي بأبعاد نانوية بحدود 10nm، قيس طيف النفاذية للمدى الطيفي (200-1200nm) ومن خلاله حسبت بعض المعلمات المهمة مثل: (معامل الامتصاص، فجوة الطاقة البصرية ومعامل الانكسار). وكذلك حسبت فجوة الطاقة (E_g) للانتقال المباشر المسموح من قياس طيف الامتصاص ووجدت ان قيمها تراوحت بين (2-2.2eV).

الكلمات المفتاحية: الأغشية الرقيقة، الكاديوم-سيلينايد، الترديد المستمر و فجوة الطاقة البصرية

Introduction

Cadmium selenide is a direct band gap semiconductor belonging to the II-IV group. Several physical and chemical techniques are employed for the deposition of CdSe thin films. CdSe thin films have been grown by many deposition methods such as thermal evaporation (Patel *et al.*, 2009), chemical path deposition (Gopakumar *et al.*, 2010), pulsed laser deposition (Perna *et al.*, 2004), electrochemical deposition (Athanasopoulou *et al.*, 2012), electron beam evaporation (Suthan *et al.* 2012), successive ionic layer adsorption and reaction (SILAR) (Saglam *et al.*, 2012) and DC-sputtering technique (Glew *et al.*, 1977).

CdSe as a semiconductor is well studied and found to be promising material for its application in the area of electronic and optoelectronic such as photo detection (Nair *et al.*, 1993), gas sensing (Patel *et al.*, 1994), thin film transistor and solar energy conversion (Chanda 2008). It is well known fact that the quality of the device based on CdSe thin films strongly depends on the structural and electronic properties of the films obtained by various experimental conditions. The material has been grown bulk, single crystalline and polycrystalline, and has been used as an efficient photo detector device.

A study was made of the preparation and properties of films sputtered from a CdSe target in a Argon gas.

Sputtering is a method for depositing very thin layers of a material onto a surface by bombarding a source material in a sealed chamber with electrons and other energetic particles to

eject atoms of the source as a form of aerosol that then settle onto all surfaces in the chamber. The process can deposit extremely fine layers of films down to the atomic scale, but also tends to be slow and is best used for small surface areas.

The aim was to produce Nano structural films with suitable properties utilizing a DC-sputtering technique.

Materials and Methods

Thin films of CdSe were deposited on chemically and ultrasonically cleaned glass substrates with the help of vacuum coating unit. Stoichiometric CdSe powder having purity around 99.99% was capsulated in a pullet shape of ($\approx 2 \times 2 \text{ cm}^2$) dimension prepared to be as electrode (Target) inside the sputtering chamber.

The attainable films thickness were calculated using "StellarNet's Thin Film measurement system" by means of optical interference method and found to be around $500 \text{ nm} \pm 5$ according to deposition conditions: (2×10^{-2} mbar inside chamber pressure, 2KV supplied voltage between the anode and cathode and 2 hour deposition period).

Results and Discussion

Structural properties

The X-ray diffraction analysis of prepared CdSe thin films have been carried out and the X-ray diffractogram have been shown in Fig.(1) and table (1). The peaks of CdSe samples have been obtained due to diffraction corresponding to (111), (101), (103), (201) reflections which is in a very good agreement with polycrystalline (hexagonal and cubic) CdSe structure,

(joint committee on diffraction standards) JCPDS card no. 19-0191, CAS No.1306-24-7. Since the thickness of the films was not sufficiently enough, the intensity of other peaks is almost negligible (very near to the noise line) this can be rectified only after setting up of the grazing angle. Since the grown films possess hexagonal structure.

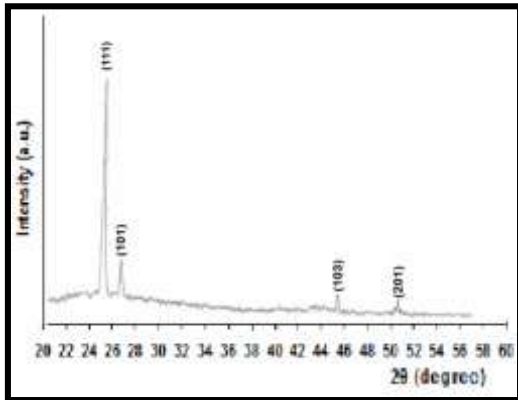


Fig.(1) X-ray Diffraction Pattern of CdSe Thin Film

Table (1) X-ray Diffraction Data for Cd Se Target

Thicknesses nm	2θ (deg)	d (Å)	hkl
500	25.414	3.5018	111
	26.794	3.324	101
	45.698	1.984	103
	50.781	1.797	201

In order to investigate the surface microstructure and quantifies the surface topography, an atomic force microscopy (AFM) technique are utilized using the instrument type (ATELISS MAITRE).

The surface morphology of the CdSe thin films observed from the AFM micrograph which confirms that the

grains are uniformly distributed within the scanning area (520nm×520nm). An initial visual realization of the deposited films on glass substrate has shown that they are compact and have good adherence to the substrate. All the CdSe films exhibit smooth surface morphology with uniform nanocrystalline CdSe grains of about 10nm and average roughness 0.2nm as shown in figure(2).

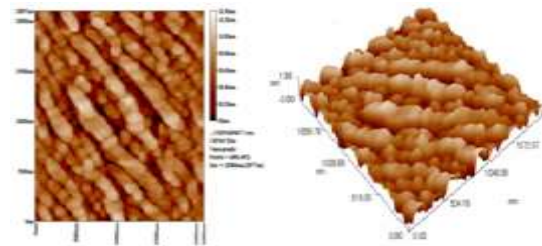


Fig.(2) The AFM Images of CdSe thin film

Optical properties

The optical absorption spectrum of CdSe films have been recorded in the wavelength range (200-1200)nm. The results of these investigations have been used for the calculations of absorption coefficients and other parameters. The calculated absorption coefficient corresponding to the energy of incident radiation has been plotted with respect to the energy of photons. The fundamental absorption, which corresponding to the transition from the valance to the conduction band, can be used to determine the band gap of the material. The relation between α and the incident photon energy ($h\nu$) can be written as :

$$(\propto h\nu) = A(h\nu - E_g)^r \dots\dots(1)$$

Where A is a constant, Eg is the band-gap of the material and the exponent (r) depends on the type of transition. The parameter (r) may have values: 1/2, 2, 3/2, 3 corresponding to the allowed direct, allowed indirect, forbidden direct and forbidden indirect transitions respectively.

The value of Eg is evaluated by extrapolating the straight line portion of $(\alpha h\nu)^2$ vs. $h\nu$ has been shown in Fig(3). The values of the direct band gap is ($>2\text{eV}$) for the CdSe thin films in present investigations is in good agreement with the reported data (M.D. Athanassopoulou).

Using absorption spectra, transmission and reflection coefficients have been computed by the equations:

$$T\% = \left(\frac{I}{I_0}\right) \times 100\% \dots\dots\dots(2)$$

$$R = 1 - (T + A) \dots\dots\dots (3)$$

The variations of A, T, R and α with wavelength have been shown in graphical form in Fig.(4 a,b,c and d respectively). It implies that the absorption and the reflection possess almost the same trend. But the value of absorption in percentile is more than that of reflection.

Furthermore, the reflectance (R) and the optical constants like the extinction coefficient (K) and the refractive index (n) at certain constant wavelength (λ) are related through the following equations:

$$k = \frac{\alpha\lambda}{4\pi} \dots\dots\dots(4)$$

$$R = \frac{(n-1)^2+k^2}{(n+1)^2+k^2} \dots\dots\dots(5)$$

Using these relations, the values of (k) and (n) have been calculated at different input wavelengths from the measurement of T & R.

The relation of the refractive index (n) and the extinction coefficient (k) with wavelength for CdSe thin films are shown in Fig. (4,e and f). The general trend of variation in these parameters is fairly the same for all the materials. For example (k) and (n) values increase gradually up to about 303nm and then decrease sharply again.

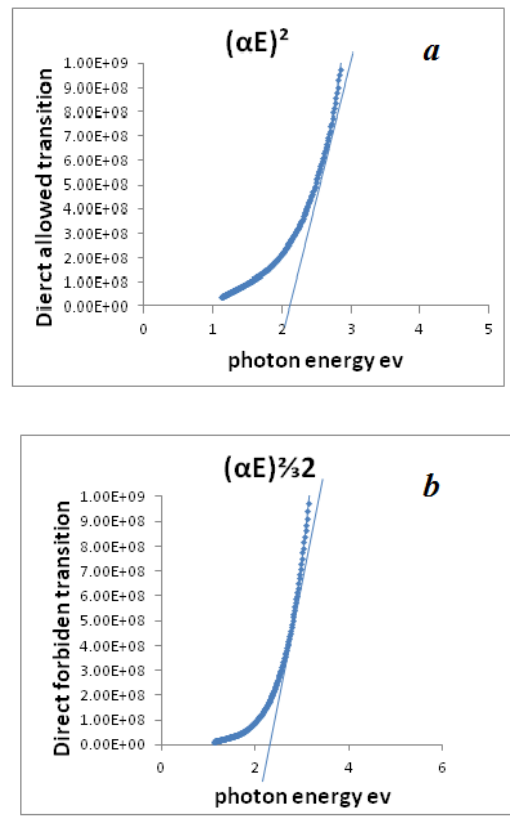
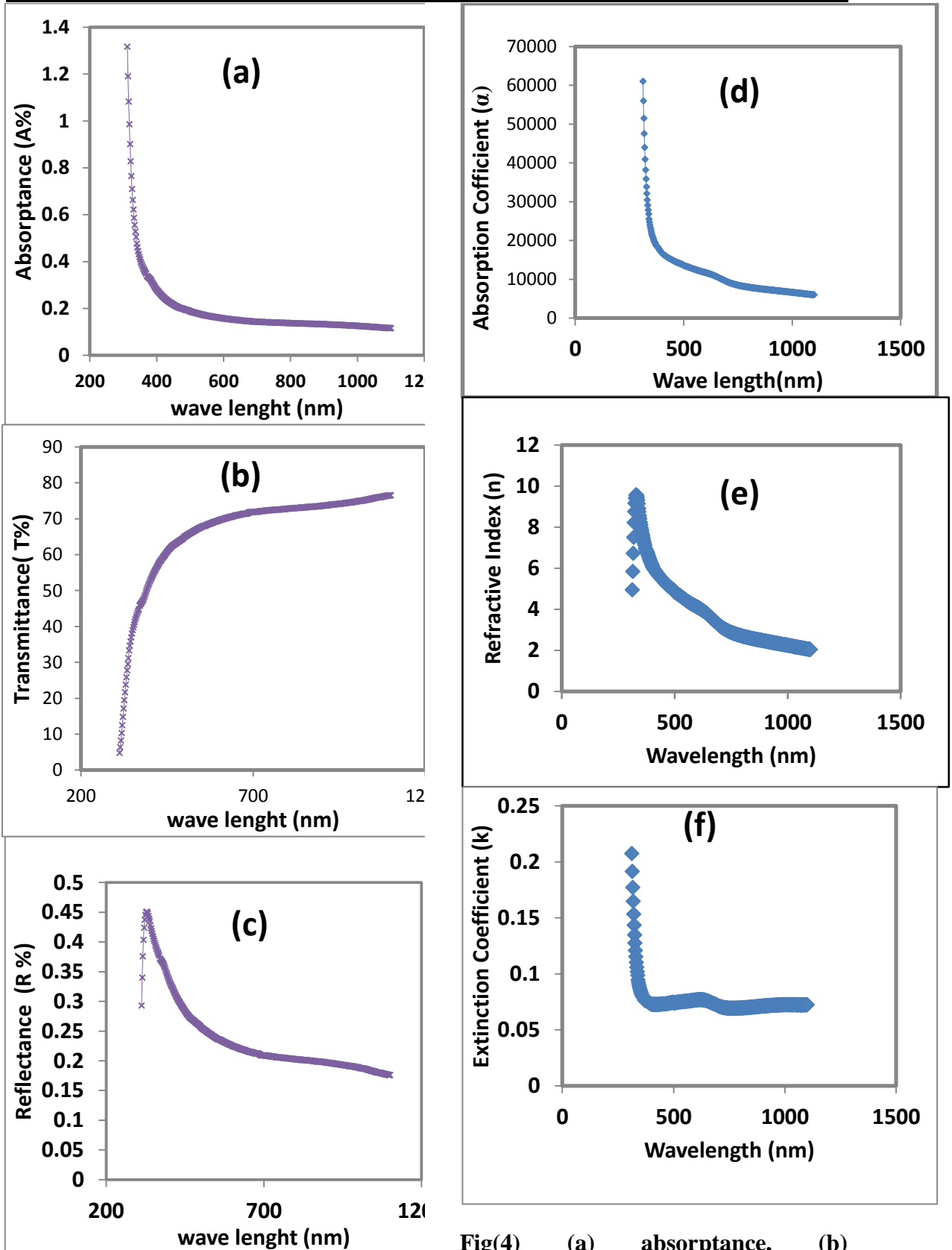


Fig. (3) The Direct Allowed (a) and the Direct Forbidden (b) Transition



Fig(4) (a) absorbance, (b) Transmittance, (d) Reflectance, (d) Absorption Coefficient, (e) Refractive Index and (f) Extinction Coefficient.

Conclusions

A very good quality, stoichiometric and epitaxial like CdSe thin films were grown on to non-conducting glass substrates using DC-sputtering method. From XRD analysis, the structural parameters like crystallite size were calculated. The results are in good agreement with the earlier reported values. From the optical studies, a very sharp absorption at 700nm was observed and the band gap was found to be around (2-2.2)eV, which suggest that sputtering deposited CdSe film is a good candidate for solar cell.

References

- Athanassopoulou, M.D.;** Mergos, J.A.; and Palaiologopoulou, M.D. (2012). Structural and Electrical Properties of Annealed CdSe Thin Solid Films..(520),6515-6520.
- Chanda, Sh.K.**(2008). Copper Doped Window Layer for CdSe Solar Cell. M.Sc. Thesis, Dept. of Electrical Eng., College of Eng., Univ. of South Florida.
- Glew, R.W.** (1977). Cadmium Selenide Sputtered Films. Thin Solid Films. (46), 59-67.
- Gopakumar, N.;** Ajana, P.S.; and VidyadharanPilla, P.K. (2010). Chemical Bath Deposition and Characterization of CdSe Thin Films for Photoelectric Applications. J. Matt.Sci. (45), 6653-6656.
- Nair, M.T.;** Nair, P.K.; Zingaro, R.A. and Meryers, E.A. (1993). Enhancement of Photoelectric in Chemically Deposited CdSe Thin Films by Air annealing J. Appl. Phys. (74), 1879-1884.
- Patel, K.D.;** Jani, M.S.; Pathak, V.M.; and Srivasava, R. (2009). Use of Cadmium Selenide Thin Films as a Carbon Dioxide Gas Sensor.. Chalcoginate Letters. (6), 279-286.
- Patel, N.G.;** Panchal, C.J. and Makhija, K.K. (1994). Deposition of CdSe Thin by Films Thermal Evaporation and Their Structural and Optical Properties. Crystal Research and Technology, 29(7), 1013-1020.
- Perna, G.;** Capozzi, V.; Ambrico, M.; Augelli, V.; Ligonzo, T.; and Minafra, A. (2004). Structural and Optical Properties Characterization of Zn Doped CdSe Films. Appl. Surf. Science. (233), 366-372.
- Saglam M;** Ates, A., Guzeldir, B., and Ozakin, O., the surface properties of the cds, cdse , cuseand znse thim Films Growth by SILAR method Proc of Int. Conf. CuS, ZnS, CdSe, CuSe and ZnSe Thin. Nanomaterials ; Applications and Properties. (1), (3) (2012).
- Suthan, N.J.;** Jayachandran, M., and Perumal, K. (2012). Structural and Optical Properties of Electrical Beam Evaporated CdSe Thin Films. Matter. Sci. 30 (6), 547-551.

Bioavailability of Ellagic Acid in Plasma of 20 Healthy Volunteers Using HPLC Technique.

**Fadl Mehseen Abid *Jasim Mohamed Salman

** Ministry of Science and Technology *Ministry of Industry and Minerals
Baghdad- Iraq

E-mail: fadlabid334@yahoo.com

Abstract

Ellagic acid (EA) and hydrolysable ellagitannins (ETs) were extracted from white flesh pomegranate; the ellagic acid was implicated with potent antioxidant, anticancer and antiatherosclerotic biological properties. ellagic acid act as excellent scavenger for chemical causing cancer , It form a layer on DNA to prevent free radicals damaging

The concentration –time curve was constructed after administration of 80 mg ellagic acid to 20 healthy volunteers (14 male and 6 females) . The calibration curve for quantification of EA was linear ($r^2 = 0.9998$) over concentration range from 400 to 6.25 ng/ml. the maximum concentration of ellagic acid (C max) was achieved in plasma of volunteers after 1 h (T max). the mean serum elimination half life was about 6.21 ± 1.35 h . The recovery of ellagic acid in plasma at different concentration from 50-400 ng/ml were between 101-117 % .

Keywords: Bioavailability , Ellagic Acid and Plasma.

قياس التوافر الحيوي لحمض اللاجيك في مصل الدم ل 20 من المتطوعين بتقنية السائل الكروماتوغرافي عالي الاداء

فاضل محسن عبد ** جاسم محمد سلمان*
** وزارة العلوم والتكنولوجيا*وزارة الصناعة والمعادن
بغداد – العراق

الخلاصة

حامض اللاجيك ومادة الاجنين المتحلل من مستخلص الشحم الابيض للرمان له فعالية واسعة كمادة مضادة للاكسدة- مضادة للسرطان، مضادة لتصلب الشرايين، اضافة الى ان حامض اللاجيك يعمل على قنص المواد الكيميائية المسببة للسرطان ويعمل طبقة رقيقة على الحامض الرايبوي لمنع تأثير الجذور الحرة. قيست علاقة التركيز بالزمن بعد اعطاء 80mg من حامض اللاجيك الى 20 متطوعين اصحاء (14 ذكر و8 اناث). كما اشارت النتائج الى ان قياس حامض اللاجيك اعطى دالة خطية للتركيز المحصورة بين (400-6.2 ng/ml) و اعلى تركيز لحمض اللاجيك بلازما الدم للمتطوعين وصلت خلال ساعة واحدة و زمن النصف ل طرح حامض اللاجيك تم الوصول اليه خلال 6.21 ± 1.35 ساعة ، النسبة المئوية لاستخلاص حامض اللاجيك المسترجع من بلازما الدم وكانت بين 101-117%.

الكلمات المفتاحية: التوافر الحيوي ، حامض اللاجيك و مصل الدم.

Introduction

The extracted polyphenols from various plants play an important role in human nutrition and are implicated with numerous biological properties including, anticancer, antioxidant, anti-inflammatory, and anti-atherosclerotic activities. (Cerda, *et al.*, 2003) Among these phytochemicals, ellagic acid (EA), which was highly available extract in white flesh pomegranate, either free ellagic acid, as EA or bound as ellagitannins (ETs) (Amakura, 2000).

The absorption, bioavailability and pharmacokinetics of EA administered orally have not been adequately investigated. (Aviram, *et al.*, 1986).

Ellagic acid has been reported to have antiviral activity and provide high protective against cancers of colon, lung, esophagus and cervical cancer. (Boukharta, *et al.*, 1992). The bioavailability and pharmacokinetic studies in human are necessary to determine the effect of these bioactive dietary polyphenols, apart from being prevalent in foods, are also commonly used as botanical ingredients in dietary and herbal supplements. (Navindra, *et al.*, 2004).

The previous knowledge on the bioavailability of EA and ETs is confined to animal studies with rats and mice (Smart, *et al.*, 2000). When mice were given ETs (from raspberries or pomegranates at 600 mg/kg body weight), EA was detected in the urine (0.05% of dose) as a result of absorption and metabolism of ETs (Belal, *et al.*, 2009).

However, virtually no EA was recovered from the blood or tissues of mice fed for 1 week on a diet containing 1% EA (Cerda, *et al.*, 2003 and Teel, *et al.*, 1988).

Following oral administration of EA to rat, 10% of the dose was excreted and detected as EA metabolites in urine and faeces (Smart, *et al.*, 2000), (Borges *et al.*, 2010).

The low levels of free EA in plasma have been attributed to its low solubility in water (Lei *et al.*, 2003)..

Furthermore may also be due to its extensive metabolic transformation and degradation prior to absorption. In addition, EA has been reported to bind irreversibly to cellular DNA and proteins which may also account for its limited transcellular absorption (Gil, *et al.*, 2001).

The poor absorption of EA has been reported to impact its *in vivo* anti-tumorigenic activity since it is possible that sufficient levels are not present in plasma or target cells after oral administration. (Ayrton *et al.*, 1992 and Whitley, *et al.*, 2003).

In this study we investigated the bioavailability and pharmacokinetics of EA in plasma of 20 healthy volunteers after oral single dose administration of 80 mg capsules to determine the concentration of EA in their body.

Materials and Methods

Twenty, nonsmoking, healthy volunteers (14 males, mean age \pm SD, 32.5 \pm 4.5 years; weight, 65.5 \pm 6.5 kg; height, 168.5 \pm 4.0 cm) and (6 females, mean age \pm SD, 28 \pm 4.5 years; weight, 54.5 \pm 4.5 kg; height, 162.5 \pm 5.5 cm) in two groups took part in this study. All volunteers gave written informed consent after they had received detailed instructions about the study performance of ellagic acid. All volunteers gave written informed consent after they had received detailed instructions about the study performance of ellagic acid. All volunteers were in good physical health according to physical examination, hematological and urinary laboratory tests. These volunteers did not take any other medications for at least 1 week prior to and throughout the study. Each volunteer fasted overnight before the experiment. Ellagic 80 mg

capsules were swallowed with 150 ml water.

A light, normal lunch consisting of cheese, bread, tea and water was given to all volunteers 4 hours after dosing.

Blood Sampling

The blood samples had been drawn from each volunteer after oral dose administration of 80 mg ellagic acid capsules, according to the randomization schedule, with 150 ml drinking water.

Blood samples (3 mL) were taken via an indwelling venous cannula at the following times: before drug administration (0 hr), and at 0.3, 1, 2, 3, 4, 6, 8, 10 and 12 hr after administration, the collected plasma transferred to labeled tubes. The EDTA blood samples were centrifuged at 3000 g for 10 min at 4°C, and the plasma was quickly removed and stored at -20°C until HPLC analyses. A 500 µl portion of plasma was adjusted to pH 2.5 with 150 µl of 1M potassium dihydrogen phosphate solution and 15 µl 50% phosphoric acid. Each sample was vortex mixed with 2.5 ml acetonitrile for 1 min and centrifuged at 3500 g for 10 min at 5-10 °C. The supernatant was evaporated to dryness at 35°C using a stream of liquid nitrogen. The residue was reconstituted in 100 µl methanol and 50µl (sample volume) was injected onto an HPLC system to determine the concentration of EA.

High-performance Liquid Chromatographic (HPLC) Analysis

Analysis was performed on Shimadzu binary liquid chromatography model LC-10AVP, the system equipped with shimadzu SPD 10 A vp UV_VIS spectrophotometers (Shimadzu ,Kyoto, Japan) , The mobile phase, solvent A 1.5% acetic acid in water and solvent B 1.5% acetic acid in methanol was used under binary linear gradient with a flow rate of 1.0 ml/min. The wavelength was

monitored at 360 nm for detection and quantification of ellagic acid EA (standard EA obtained from Sigma, USA), typical chromatogram for standard EA is shown in Fig. 2 , the retention of Ea in chromatogram is 6.10 min.

EA standard(50µg/ml) was solubilized in DMSO and serially diluted to prepared 400, 200, 100, 50, 25 and 12.5 ng/ml solutions. Control plasma was spiked with individual solutions and extracted as previously outlined. Each plasma sample was separately extracted (x 3) and each sample was injected in triplicate on the HPLC. Concentrations were determined from the peak area by using the equation for linear regression obtained from the calibration curve. The calibration curve was linear (R = 0.9998) over the concentration range from 400 to 12.5 ng/ml. as shown in fig 1. The recoveries of EA from human plasma were 101, 107, 104 and 112 % for the concentrations 400, 200, 100, and 50 ng/ml, respectively.

The method was linear over a range of 12.5 – 400 ng/ml of ellagic acid in plasmas.

Pharmacokinetics and Metabolism

Following oral administration of ellagic acid capsule 80 mg, the maximum peak plasma concentrations of EA occur within about 1 hours, the concentration of EA from extracted plasma samples, with different time interval from 0-12 h, were measured and tabulated in table 1.

To compare the rate and extent of absorption of EA solutions, the following pharmacokinetic variables were calculated for each volunteer using actual blood sampling times. The areas under the plasma concentration-time curves (AUC 0-12 hr) were calculated using the linear trapezoidal rule. The maximum plasma concentration (C_{max}) and time to reach maximum plasma concentration (T_{max}) were obtained

directly from the plasma-concentration data.

The elimination rate constant was calculated by least-squares regression

using the last points of each curve; the pharmacokinetics parameter for EA was summarized in table 2.

Table (1) Mean Concentration of Ellagic Acid (ng/ml) in Plasma of 20 Healthy Volunteers after Oral Dose of 80 mg Ellagic Acid Capsule.

no	Time hours								
	0.0	0.3	1	2	3	5	7	9	12
1	0	172	320	190	170	121	90	50	12.5
2	0	179	311	188	162	117	80	44	Nd
3	0	182	341	192	171	123	88	34	Nd
4	0	191	299	185	172	131	93	36	15
5	0	182	309	173	168	120	81	52	Nd
6	0	162	317	205	164	95	72	62	16
7	0	175	295	196	172	132	92	66	Nd
8	0	159	362	219	178	134	98	42	Nd
9	0	194	314	222	162	127	77	50	Nd
10	0	177	309	172	178	125	82	41	16
11	0	182	312	195	162	121	90	43	20
12	0	166	279	201	157	110	71	36	Nd
13	0	180	289	207	155	126	82	42	Nd
14	0	178	370	219	165	116	99	54	Nd
15	0	166	361	195	169	112	82	46	Nd
16	0	194	352	186	142	124	75	40	Nd
17	0	179	338	176	159	132	65	36	18
18	0	181	369	182	165	124	73	38	17
19	0	192	295	209	160	136	70	45	Nd
20	0	187	272	202	150	124	62	41	Nd
Mean	0	178.9	320.7	204.35	164.05	122.5	81.10	44.9	-
±SD	0	7.945	15.035	9.2175	7.2025	5.125	3.055	1.245	-

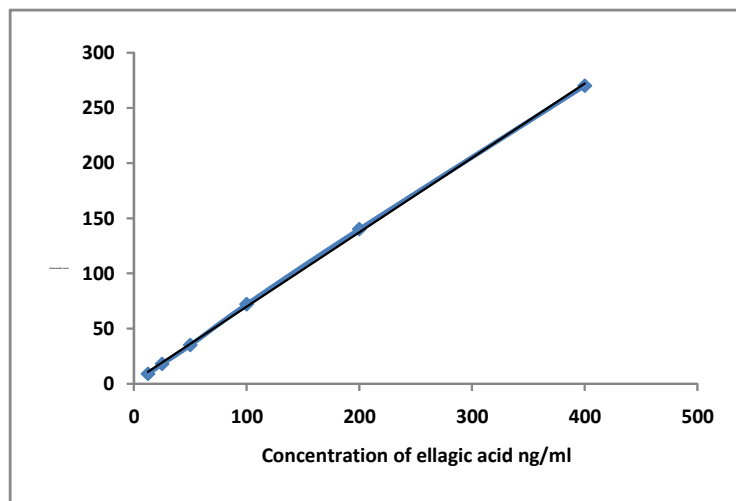


Fig. (1) Calibration Curve of Ellagic Acid

Results and Discussion

The optimum separation condition previously reported (Whitley.*et al* .2003) were modified by using fast liquid chromatographic column (50 mm length instead of 250 mm ,using high surface area ,3 μ m particle size , the retention time R_t ellagic acid standard was 6.10 min Fig 2A, while the control plasma showed no corresponding peaks detected in the plasma sample (Fig. 2B) . However since EA was detected, control plasma was spiked with different concentrations of EA standard and processed according to the extraction procedure for quantification purposes. Fig 2 C shows the EA peak eluting at 6.06 min in spiked control plasma. EA was detected and quantified in plasma

samples collected at 0.3h -12 h as shown in table 1. From this table, we clearly observed that most EA was not detected in plasma samples collected at 12h after oral administration. The concentration –time curve fig 3, Show that, the maximum absorption was achieved in 1 h, with maximum concentration of 320.7 ng/ml and half life was 6.12 h. this information is very important for estimation the dose and therapeutic concentration for various applications.

In conclusion, by combining an extraction procedure for plasma sample preparation and an HPLC-UV system, we have successfully obtained direct evidence of the absorption of EA in human plasma as data base for further studies related therapeutic effect of EA on cancer cells.

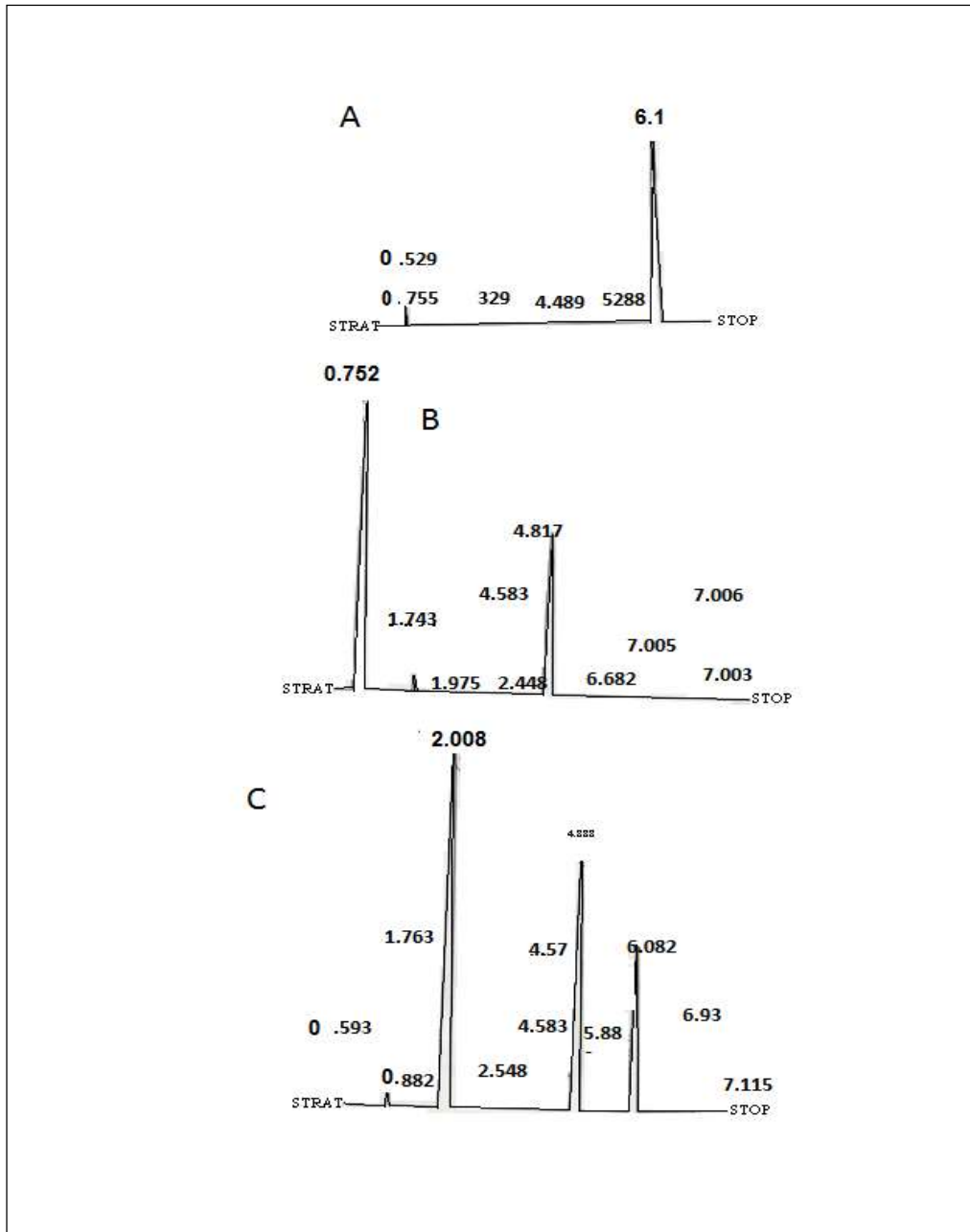


Fig. (2) Typical Chromatogram of (A) Standard Ellagic Acid Separated by Applied the Optimal Condition in the Text. (B) Blank Plasma Free Ellagic Acid , (C) Plasma from Patient after Oral Dose of 80mg of Ellagic Acid Rt=6.1 .

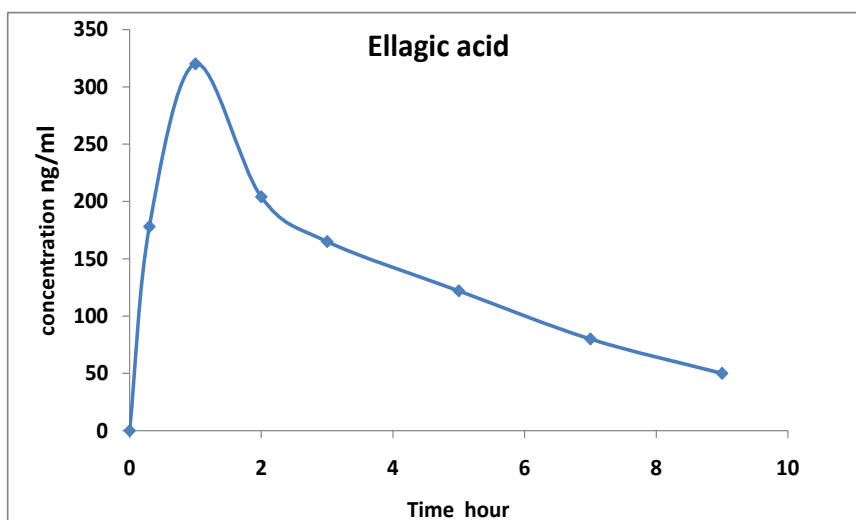


Fig. (3) Mean Plasma Concentration-time Curve of Ellagic After Oral Administration of 80 mg to 20 Healters. Volunteer

Table (2) Mean value of Pharmacokinetic Parameters of Single Dose Administration of 80 mg Ellagic Acid to 20 Healthy Volunteers.

Subje ct No.	K_a	$K_a 0.5t$	$K_{elem.}$	K_{elem} 0.5t	C_{max}	T_{max}	AUC
Mean	7.24	0.156	0.092	6.20	320.7	1.0	1623.7
\pm SD	0.67	0.017	0.021	1.20	22.56	0.0	121.95

K_a : Time of Absorption,

$K_a 0.5t$: Half time of Absorption

K_{elem} : Time of Elimination

$K_{elem} 0.5t$: Half Time of Elimination

C_{max} : Maximum Concentration

T_{max} : Maximum Time to Reach Maximum Concentration

AUC: Area Under Curve

References

- Amakura, Y.;** Okada, M.; Tsuji, A.; and Tonogai, Y.;(2000).“High-performance Liquid Chromatography Determination with Photodiode Array Detection of Ellagic Acid in Fresh and Processed Fruits. J. And ChromatogB”. 896, 87-93.
- Aviram, M.** and Dornfield, L.(1986); “Pomegranate Juice Consumption of the Naturally Occurring Antimutagenic Plant Phenol, Ellagic Acid, and its Synthetic Derivatives, 3-O-decylellagic Acid and 3,3-di-O-Methylellagic Acid in Mice. Carcinogenesis”. 7,1663-67.
- Ayrton** and Lewis, D.F.V. (1992). Antimutagenicity of Ellagic Acid Toward the Food Mutagen IQ: Investigations Into the Possible Mechanisms of Action. Food Chem Toxicol”. 30,289-95.
- Belal, S.K. M;** Abedl-Rahman, A.H., Mohamed, D.S and Osman, H; (E2009). “Protective Effect of Pomegranate Fruit Juice Against Aeromonas Hydrophila Induced Intestinal Histopathological Test in Mice, World. Appl .Sci.J, 7,245-254.
- Borges, G.;** Degeneve, A. ; Mullen, W.; And Crozier A.M; (2010). “Identification of Flavonoid and Phenolic Antioxidants in Balkan Currants ,Blueberries, Raspberries, "Red Currants and Cranberries,, J Agri.Food Chem”. 58, DOI0: 1021/jf902263n.
- Boukharta ,M.;**Jalbert, G.;Castonguay, (1992). “A. Efficacy of Ellagitannins and Ellagic Acid as Cancer Chemopreventive Agents. Proc XVIth Int Conf of the Groupe Polyphénols, Lisbon”, 245-49.
- Cerda, B.;** Ceron, J.J.;. Tomas-Barberan F.A And Espin; J.C.(2003). “Repeated Oral Administration of High Doses of Pomegranate Ellagitannin Punicalagin to Rats for 37 Days is Not Toxic. J Agric Food Chem”. 51,3493-501.
- Cerda, B.;** Llorach ,R.; Ceron, J.J.; Espin J.C. and Tomas-Barberan F.A. (2003). “Evaluation of the Bioavailability and Metabolism in the Rat of Punicalagin, an Antioxidant Polyphenol from Pomegranate Juice. Eur J Nutr”. 42,18-28.
- Gil, M.I.;** Tomas-Barberan F.A.; Hess-Pierce B., Kader A.A. (2001). “Antioxidant Activity of Pomegranate Juice and Its Relationship with Phenolic Composition and Processing. Inhibits Serum Angiotensin Converting Enzyme Activity and Reduces Systolic Blood Pressure. Atherosclerosis 158,195-98.
- Lei, F. X. Xing,D.M.;** Xiang and Zhao.L, (2003). Pharmacokinetic Study of Ellagic Acid in Rat After Oral Administration of Pomegranate leaf Extract. J. Chrom B .796,189-94.
- Navindra, P.;** Seeram, R.L., and David, H.:(2004). “Bioavailability of Ellagic acid in Human Plasma after Consumption of Ellagitannins from Pomegranate (*Punica granatum* L.) Juice., Clinica Chimica Acta, in Press
- Smart, R.C.;** Huang, M.T.; Chang, R.L. and Sayer ,J.M.; (2000). “Disposition Agric Food Chem”. 48,4581-89.
- Teel, R.W.;** Martin R.M. (1988). Disposition of the Plant Phenol Ellagic Acid in the Mouse Following Oral Administration by Gavage. Xenobiotica 18,397-405.
- Whitley, A.C.;** Stoner, G.D.; Darby, M.V. Walle, T and (2003). Intestinal Epithelial Cell Accumulation of Cancer Preventive Polyphenol Ellagic Acid-extensive Binding to Protein and DNA. Biochem Pharmacol;66, 907-15.